# Atmospheric Dynamics

# 7

This chapter introduces a framework for describing and interpreting the structure and evolution of large-scale atmospheric motions, with emphasis on the extratropics. We will be considering motions with horizontal scales[1] of hundreds of kilometers or longer, vertical scales on the order of the depth of the troposphere, and timescales on the order of a day or longer. Motions on these scales are directly and strongly influenced by the Earth's rotation, they are in hydrostatic balance, and the vertical component of the three-dimensional velocity vector is nearly four orders of magnitude smaller than the horizontal component but is nonetheless of critical importance. The first section introduces some concepts and definitions that are useful in characterizing horizontal flow patterns. It is followed by a more extensive section on the dynamics of large-scale horizontal motions on a rotating planet. The third section introduces the system of *primitive equations*, which is widely used for predicting how large-scale motions evolve with time. The chapter concludes with brief discussions of the atmospheric general circulation and numerical weather prediction.

## 7.1 Kinematics of the Large-Scale Horizontal Flow

*Kinematics* deals with properties of flows that can be diagnosed (but not necessarily predicted) without recourse to the equations of motion. It provides a descriptive framework that will prove useful in interpreting the horizontal equation of motion introduced in the next section.

On any "horizontal" surface (i.e., a surface of constant geopotential $\Phi$, pressure $p$, or potential temperature $\theta$), it is possible to define a set of *streamlines* (arbitrarily spaced lines whose orientation is such that they are everywhere parallel to the horizontal velocity vector $\mathbf{V}$ at a particular level and at a particular instant in time) and *isotachs* (contours of constant scalar wind speed $V$) that define the position and orientation of features such as jet streams. At any point on the surface one can define a pair of axes of a system of *natural coordinates* $(s, n)$, where $s$ is arc length directed downstream along the local streamline, and $n$ is distance directed normal to the streamline and toward the left, as shown in Fig. 7.1. It follows that at any point in the flow, the scalar wind speed

$$V = \frac{ds}{dt} \text{ and } \frac{dn}{dt} = 0$$

The direction of the flow at any point is denoted by the angle $\psi$, which is defined relative to an arbitrary reference angle. The unit vector $\mathbf{s}$ is in the local downstream direction and $\mathbf{n}$ is in the transverse direction.

### 7.1.1 Elementary Kinematic Properties of the Flow

At any point in the flow it is possible to define the kinematic properties listed in Table 7.1, all of which have units of inverse time ($s^{-1}$). The topmost four rows are elementary properties or building blocks that have precise mathematical definitions in natural coordinates. *Shear* is defined as the rate of change of

[1] The *scale* of the motions denotes the distance over which scalar fields, such as pressure or the meridional wind component, vary over a range comparable to the amplitude of the fluctuations. For example, the horizontal scale of a one-dimensional sinusoidal wave along a latitude circle is on the order of $1/2\pi$ wavelength and the scale of a circular vortex is on the order of its radius.

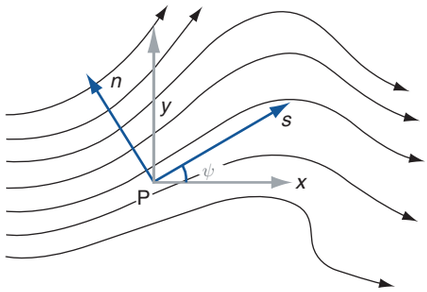


**Fig. 7.1** Natural coordinates ($s$, $n$) defined at point P in a horizontal wind field. Curved arrows represent streamlines.

the velocity in the direction transverse to the flow. *Curvature* is the rate of change of the direction of the flow in the downstream direction. Shear and curvature are labeled as *cyclonic* *(anticyclonic)* and are assigned a positive (negative) algebraic sign if they are in the sense as to cause an object in the flow to rotate in the same (opposite) sense as the Earth's rotation $\Omega$, as viewed looking down on the pole. In other words, *cyclonic* means counterclockwise in the northern hemisphere and clockwise in the southern hemisphere. *Diffluence*/*confluence* is the rate of change of the direction of the flow in the direction transverse to the motion, defined as positive if the streamlines are spreading apart in the downstream direction. *Dilation*/*contraction* relates to the rate of change of the speed of the flow in the downstream direction, with stretching defined as positive.

### 7.1.2 Vorticity and Divergence

Vorticity and divergence are scalar quantities that can be defined not only in natural coordinates, but also in Cartesian coordinates ($x$, $y$) and for the horizontal wind vector $\mathbf{V}$. *Vorticity* is the sum of the shear and the curvature, taking into account their algebraic signs, and *divergence* is the sum of the diffluence and the stretching.

It can be shown that *vorticity* $\zeta$ is given by

$$\zeta = 2\omega \tag{7.1}$$

where $\omega$ is the rate of spin of an imaginary puck moving with the flow. This relationship is illustrated in the following exercise for the special case of solid body rotation.

***Exercise 7.1*** Derive an expression for the vorticity distribution within a flow characterized by counterclockwise solid body rotation with angular velocity $\omega$ (see Fig. 7.2b).

***Solution:*** Vorticity is the sum of the shear and the curvature. Using the definitions in Table 7.1, the shear contribution is $-\partial V/\partial n = \partial V/\partial r$, where $r$ is radius in polar coordinates, centered on the axis of rotation. In one circuit $\psi$ rotates through angle $2\pi$. Therefore, the curvature contribution $V\partial\psi/\partial s = V(2\pi/2\pi r) = V/r$. For solid body rotation with angular

**Table 7.1** Definitions of properties of the horizontal flow [a]

| | Vectorial | Natural coords. | Cartesian coords. |
|---|---|---|---|
| *Shear* | | $\dfrac{\partial V}{\partial n}$ | |
| *Curvature* | | $V\dfrac{\partial \psi}{\partial s}$ | |
| *Diffluence* | | $V\dfrac{\partial \psi}{\partial n}$ | |
| *Stretching* | | $\dfrac{\partial V}{\partial s}$ | |
| *Vorticity* $\zeta$ | $\mathsf{k}\cdot\nabla\times\mathsf{V}$ | $V\dfrac{\partial \psi}{\partial s}-\dfrac{\partial V}{\partial n}$ | $\dfrac{\partial v}{\partial x}-\dfrac{\partial u}{\partial y}$ |
| *Divergence* $\mathrm{Div}_H\mathsf{V}$ | $\nabla\cdot\mathsf{V}$ | $V\dfrac{\partial \psi}{\partial n}-\dfrac{\partial V}{\partial s}$ | $\dfrac{\partial u}{\partial x}-\dfrac{\partial v}{\partial y}$ |
| *Deformation* | | $-V\dfrac{\partial \psi}{\partial n}-\dfrac{\partial V}{\partial s}$ | $\dfrac{\partial u}{\partial x}-\dfrac{\partial v}{\partial y};\dfrac{\partial u}{\partial x}+\dfrac{\partial v}{\partial y};$ |

[a] The signs of properties relating to vorticity are defined as positive for the northern hemisphere.

velocity $\omega$ the contribution from the shear is therefore $d(\omega r)/dr = \omega$ and the contribution from the curvature is $\omega r/r = \omega$. The shear and curvature contributions are in the same sense and therefore additive. Hence, $\zeta = 2\omega$. ■

Divergence $\nabla \cdot \mathbf{V}$ (or $\mathrm{Div}_H\mathbf{V}$) is related to the time rate of change of area. Consider a block of fluid of area $A$, moving downstream in the flow. In Cartesian $(x, y)$ coordinates, the Lagrangian time rate of change is

$$\frac{dA}{dt} = \frac{d}{dt}\delta x \delta y = \delta y \frac{d}{dt}\delta x + \delta x \frac{d}{dt}\delta y$$

If the dimensions of the block are very small compared to the space scale of the velocity fluctuations, we may write

$$\frac{d}{dt}(\delta x) = \delta u = \frac{\partial u}{\partial x}\delta x$$

where the partial derivative $\partial/\partial x$ in this expression indicates that the derivative is taken at constant $y$. The time rate of change of $\delta y$ can be expressed in an analogous form. Substituting for the time derivatives in the expression for $dA/dt$, we obtain

$$\frac{dA}{dt} = \delta x \delta y \frac{\partial u}{\partial x} + \delta x \delta y \frac{\partial v}{\partial y}$$

Dividing both sides by $\delta x \delta y$ yields

$$\frac{1}{A}\frac{dA}{dt} = \frac{\partial u}{\partial x} + \frac{\partial v}{\partial y} \tag{7.2}$$

where the right-hand side may be recognized as the Cartesian form of the divergence in Table 7.1. Hence, *divergence is the logarithmic rate of expansion of the area enclosed by a marked set of parcels moving with the flow*. Negative divergence is referred to as *convergence*.

Some of the relationships between the various kinematic properties of the horizontal wind field are illustrated by the idealized flows shown in Fig. 7.2.

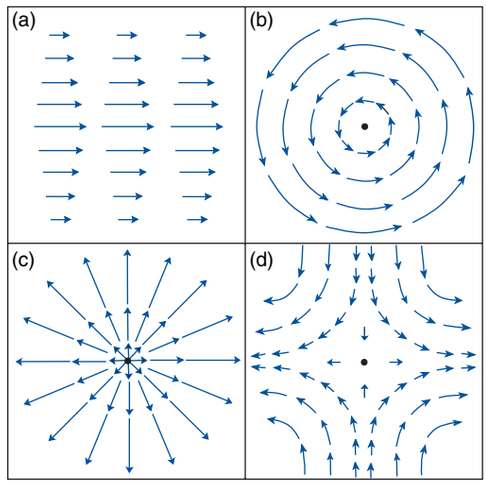


**Fig. 7.2** Idealized horizontal flow configurations. See text for explanation.

(a) Sheared flow without curvature, diffluence, stretching, or divergence. From a northern hemisphere perspective, shear and vorticity are cyclonic in the top half of the domain and anticyclonic in the bottom half.

(b) Solid body rotation with cyclonic shear and cyclonic curvature (and hence, cyclonic vorticity) throughout the domain, but without diffluence or stretching, and hence without divergence.

(c) Radial flow with velocity directly proportional to radius. This flow exhibits diffluence and stretching and hence divergence, but no curvature or shear and hence no vorticity.

(d) Hyperbolic flow that exhibits both diffluence and stretching, but is nondivergent because the two terms exactly cancel. Hyperbolic flow also exhibits both shear and curvature, but is irrotational (i.e., vorticity-free) because the two terms exactly cancel.

Vorticity is related to the line integral of the flow along closed loops. >From Stokes' theorem, it follows that

$$C \equiv \oint V_s ds = \iint \zeta dA \tag{7.3}$$

where $V_s$ is the component of the velocity along the arc $ds$ (defined as positive when circulating around the loop in the same sense as the Earth's rotation), and $C$ is referred to as the *circulation* around the loop. The term on the right hand side can be rewritten as $\bar{\zeta} A$, where $\bar{\zeta}$ is the spatial average of the vorticity within the loop and $A$ is the area of the loop. The

analogous relationship for the component of the velocity $V_n$ outward across the curve is

$$\oint V_n ds = \iint \mathrm{Div}_H \, \mathbf{V} dA \tag{7.4}$$

which follows from Green's theorem.

***Exercise 7.2*** At the 300-hPa (~10 km) level along 40 °N during winter the zonally averaged zonal wind $[u]$ is eastward at 20 m s$^{-1}$ and the zonally averaged meridional wind component $[v]$ is southward at 30 cm s$^{-1}$. Estimate the vorticity and divergence averaged over the polar cap region poleward of 40 °N.

***Solution:*** Based on (7.3), the vorticity averaged over the polar cap region is given by

$$\bar{\zeta} = \frac{[u]\oint_{40°\mathrm{N}} ds}{\iint_{40°\mathrm{N}} dA} = \frac{2\pi R_E [u] \cos 40°}{2\pi R_E^2 \int_{40°}^{90°} \cos\phi d\phi}$$

$$= \frac{[u]}{R_E} \frac{\cos 40°}{(1 - \sin 40°)} = 3.74 \times 10^{-6}\,\mathrm{s}^{-1}.$$

In a similar manner, the divergence over the polar cap region is given by

$$\overline{\mathrm{Div}_H \mathrm{V}} = \frac{-[v]\oint_{40°\mathrm{N}} ds}{\iint_{40°\mathrm{N}} dA} \frac{-[v]}{R_E} \frac{\cos 40°}{(1 - \sin 40°)}$$

$$= 5.61 \times 10^{-7}\mathrm{s}^{-1}$$ ■

### 7.1.3 Deformation

*Deformation*, defined in the bottom line of Table 7.1, is the sum of the confluence and stretching terms. If the deformation is positive, grid squares oriented along the ($s$, $n$) axes will tend to be deformed into rectangles, elongated in the $s$ direction. Conversely, if the deformation is negative, the squares will be deformed into rectangles elongated in the direction transverse to the flow. In Cartesian coordinates, the *deformation tensor* is made up of two components: the first relating to the stretching and squashing of grid squares aligned with the $x$ and $y$ axes, and the second with grid squares aligned at an angle of 45° with respect to the $x$ and $y$ axes. Figure 7.2(d) shows an example of a horizontal wind pattern consisting of pure deformation in the first component. Here the $x$ axis corresponds to the *axis of dilatation* (or stretching) and the $y$ axis corresponds to the *axis of contraction*. If this wind pattern were rotated by 45° relative to the $x$ and $y$ axes, the deformation would be manifested in the second component: rectangles would be deformed into rhomboids.

Figure 7.3 illustrates how even a relatively simple large-scale motion field can distort a field of passive tracers, initially configured as a rectangular grid, into an elongated configuration in which the individual grid squares are stretched and squashed beyond recognition. Some squares that were initially far apart end up close together, and vice versa.

Deformation can sharpen preexisting horizontal gradients of temperature, moisture, and other scalar

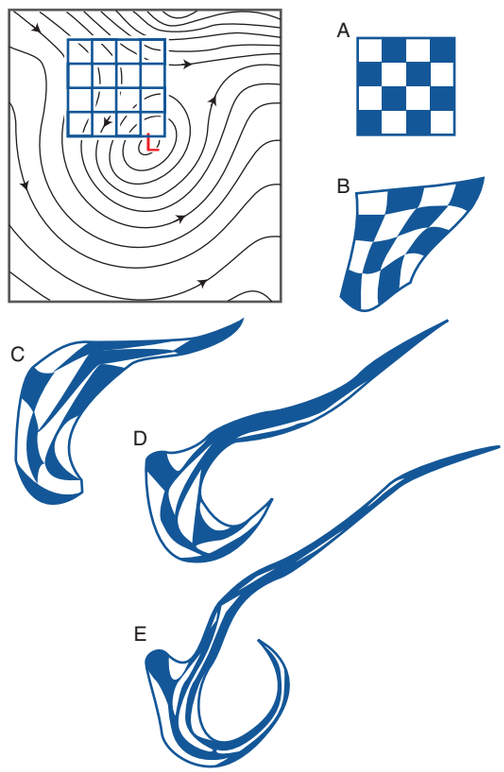


**Fig. 7.3** (Top) A grid of air parcels embedded in a steady state horizontal wind field indicated by the arrows. The strength of the wind at any point is inversely proportional to the spacing between the contours at that point. (A–E) How the grid is deformed by the flow as the tagged particles move downstream; those in the upper right corner of the grid moving eastward and those in the lower left corner moving southward and then eastward around the closed circulation. [From *Tellus*, 7, 141–156 (1955).]

variables, creating features referred to as *frontal zones*. To illustrate how this sharpening occurs, consider the distribution of a hypothetical *passive tracer*, whose concentration $\psi(x, y)$ is conserved as it is carried around (or *advected*) in a divergence-free horizontal flow. Because $d\psi/dt = 0$ in (1.3), it follows that the time rate of change at a fixed point in space is given by the horizontal advection; that is

$$\frac{\partial \psi}{\partial t} = -\mathbf{V} \cdot \nabla \psi \tag{7.5a}$$

or, in Cartesian coordinates,

$$\frac{\partial \psi}{\partial t} = -u\frac{\partial \psi}{\partial x} - v\frac{\partial \psi}{\partial y} \tag{7.5b}$$

The time rate of change of $\psi$ at a fixed point $(x, y)$ is positive if $\psi$ increases in the upstream direction in which case, $\mathbf{V}$ at $(x, y)$ must have a component directed *down* the gradient of $\psi$; hence the minus signs in (7.5a,b).

Suppose that $\psi$ initially exhibits a uniform horizontal gradient, say from north to south. Such a gradient will tend to be sharpened within regions of negative $\partial v/\partial y$. In the pattern of pure deformation in Fig, 7.2d, $\partial v/\partial y$ is negative throughout the domain. Such a flow will tend to sharpen any preexisting north–south temperature gradient, creating an east–west oriented frontal zone, as shown in Fig. 7.4a. Frontal zones can also be twisted and sharpened by the presence of a wind pattern with shear, as shown in Fig. 7.4b.

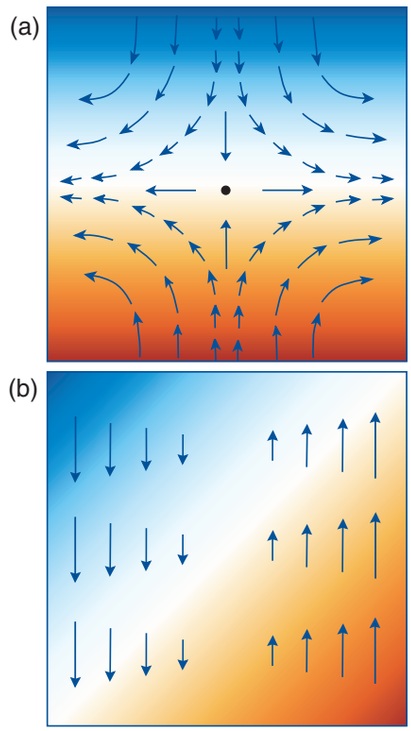


**Fig. 7.4** Frontal zones created by horizontal flow patterns advecting a passive tracer with concentrations indicated by the colored shading. In (a) the gradient is being sharpened by deformation, whereas in (b) it is being twisted and sharpened by shear. See text and Exercise 7.11 for further explanation.

### 7.1.4 Streamlines versus Trajectories

If the horizontal wind field $\mathbf{V}$ is changing with time, the *streamlines* of the instantaneous horizontal wind field considered in this section are not the same as the *horizontal trajectories* of air parcels. Consider, for example, the case of a sinusoidal wave that is propagating eastward with phase speed $c$, superimposed on a uniform westerly flow of speed $U$, as depicted in Fig. 7.5. The solid lines represent horizontal streamlines at time $t$, and the dashed lines represent the horizontal streamlines at time $t + \delta t$, after the wave has moved some distance eastward. The trajectories originate at point A, which lies in the trough of the wave at time $t$. If the westerly flow matches the rate of eastward propagation of the wave, the parcel will remain in the wave trough as it moves eastward, as indicated by the straight trajectory AC. If the westerly flow through the wave is faster than the rate of propagation of the wave (i.e., if $U > c$), the air parcel will overtake the region of southwesterly flow ahead of the trough and drift northward, as indicated by the

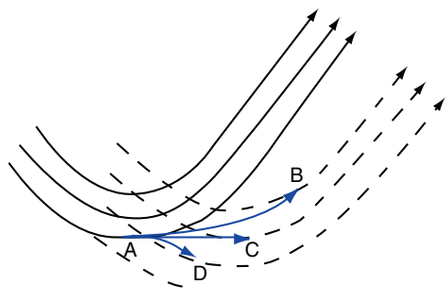


**Fig. 7.5** Streamlines and trajectories for parcels in a wave moving eastward with phase velocity $c$ embedded in a westerly flow with uniform speed $U$. Solid black arrows denote initial streamlines and dashed black arrows denote later streamlines. Blue arrows denote air trajectories starting from point A for three different values of $U$. AB is the trajectory for $U > c$; AC for $U = c$, and AD for $U < c$.

trajectory AB. Conversely, if $U < c$, the air parcel will fall behind the trough of the wave and curve southeastward, as indicated by AD. By construction, each of the three trajectories is parallel to the initial streamline passing through point A and to the respective later streamlines passing through points B, C, and D. The longest trajectory (AB) corresponds to the highest wind speed.

## 7.2 Dynamics of Horizontal Flow

Newton's second law states that in each of the three directions in the coordinate system, the acceleration $a$ experienced by a body of mass $m$ in response to a resultant force $\Sigma F$ is given by

$$a = \frac{1}{m}\sum F \tag{7.6}$$

This relationship describes the motion in an inertial (nonaccelerating) frame of reference. However, it is more generally applicable, provided that *apparent forces* are introduced to compensate for the acceleration of the coordinate system. In a rotating frame of reference two different apparent forces are required: a *centrifugal force* that is experienced by all bodies, irrespective of their motion, and a *Coriolis force* that depends on the relative velocity of the body in the plane perpendicular to the axis of rotation (i.e., in the plane parallel to the equatorial plane).

### 7.2.1 Apparent Forces

The force per unit mass that is referred to as *gravity* or *effective gravity* and denoted by the symbol $g$ represents the vectorial sum of the true gravitational attraction $g^*$ that draws all elements of mass toward Earth's center of mass and the much smaller apparent force called the *centrifugal force* $\Omega^2 R_A$, where $\Omega$ is the rotation rate of the coordinate system in radians per second (i.e., $s^{-1}$) and $R_A$ is the distance from the axis of rotation. The centrifugal force pulls all objects outward from the axis of planetary rotation, as indicated in Fig. 7.6. In mathematical notation, $g = \mathbf{g}^* + \Omega^2\mathbf{R_A}$.

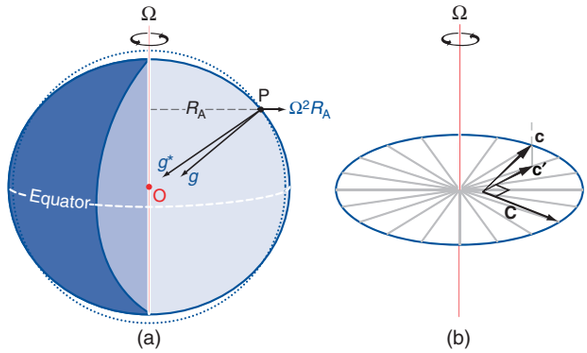


**Fig. 7.6** (a) Apparent forces. Effective gravity $g$ is the vectorial sum of the true gravitational acceleration $g^*$ directed toward the center of the Earth O and the *centrifugal force* $\Omega^2 R_A$. The acceleration $g$ is normal to a surface of constant geopotential, an oblate spheroid, depicted as the outline of the Earth. The dashed reference line represents a true spherical surface. (b) The Coriolis force C is linearly proportional to c′ to the component of the relative velocity c in the plane perpendicular to the axis of rotation. When viewed from a northern hemisphere perspective, C is directed to the right of c′ and lies entirely within the plane perpendicular to the axis of rotation.

Surfaces of constant geopotential $\Phi$, which are normal to **g**, are shaped like oblate spheroids, as indicated by the outline of the Earth in Fig. 7.6. Because the surface of the oceans and the large-scale configuration of the Earth's crust are incapable of resisting any sideways pull of effective gravity, they have aligned themselves with surfaces of constant geopotential. A body rotating with the Earth has no way of separately sensing the gravitational and centrifugal components of effective gravity. Hence, the $\Omega^2\mathbf{R_A}$ term is incorporated into **g** in the equations of motion.

An object moving with velocity **c** in the plane perpendicular to the axis of rotation experiences an additional apparent force called the *Coriolis*[2] *force* $-2\Omega \times \mathbf{c}$. This apparent force is also in the plane perpendicular to the axis of rotation, and it is directed transverse to the motion in accordance with the right hand rule (i.e., if the rotation is counterclockwise when viewed from above, the force is directed to the right of **c** and vice versa).

When the forces and the motions are represented in a spherical coordinate system, the horizontal component of the Coriolis force arising from the

[2] **G. G. de Coriolis** (1792–1843) French engineer, mathmatician, and physicist. Gave the first modern definition of kinetic energy and work. Studied motions in rotating systems.

horizontal motion **V** can be written in vectorial form as

$$\mathbf{C} = -f\mathbf{k} \times \mathbf{V} \tag{7.7}$$

where $f$, the so-called *Coriolis parameter*, is equal to $2\Omega \sin \phi$ and **k** is the local vertical unit vector, defined as positive upward. The $\sin \phi$ term in $f$ appropriately scales the Coriolis force to account for the fact that the local vertical unit vector **k** is parallel to the axis of rotation $\Omega$ only at the poles. Accordingly, the Coriolis force in the horizontal equation of motion increases with latitude from zero on the equator to $2\Omega V$ at the poles, where $V$ is the (scalar) horizontal wind speed. The Coriolis force is directed toward the right of the horizontal velocity vector in the northern hemisphere and to the left of it in the southern hemisphere. On Earth

$$\Omega \equiv 2\pi \text{ rad day}^{-1} = 7.292 \times 10^{-5} \text{ s}^{-1}$$

where *day* in this context refers to the *sidereal day*,[3] which is 23 h 56 min in length.

### 7.1 Experiment in a Dish

The role of the Coriolis force in a rotating coordinate system can be demonstrated in laboratory experiments. Here we describe an experiment that makes use of a special apparatus in which the centrifugal force is incorporated into the vertical force called gravity, as it is on Earth. The apparatus consists of a shallow dish, rotating about its axis of symmetry as shown in Fig. 7.7. The rotation rate $\Omega$ is tuned to the concavity of the dish such that at any given radius the outward-directed centrifugal force exactly balances the inward-directed component of gravity along the sloping surface of the dish; that is

$$g\frac{dz}{dr} = \Omega^2 r$$

where $z$ is the height of the surface above some arbitrary reference level, $r$ is the radius, and $\Omega$ is the rotation rate of the dish. Integrating from the center out to radius $r$ yields the parabolic surface

$$z = \frac{\Omega^2 r^2}{2g} + \textit{constant}$$

The constant of integration is chosen to make $z = 0$ the level of the center of the dish.

Consider the horizontal trajectory of an idealized frictionless marble rolling around in the dish, as represented in both a fixed (inertial) frame of reference and in a frame of reference rotating with the dish. (To view the motion in the rotating frame of reference, the video camera is mounted on the turntable.)

In the fixed frame of reference the differential equation governing the horizontal motion of the marble is

$$\frac{d^2 r}{dt^2} = -\Omega^2 r$$

It follows from the form of this differential equation that the marble will execute ellipsoidal trajectories, symmetric about the axis of rotation, with

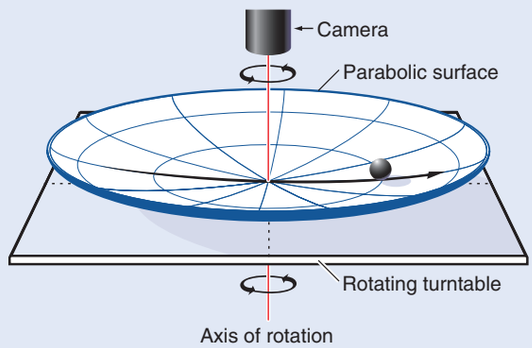


**Fig. 7.7** Setup for the rotating dish experiment. Radius $r$ is distance from the axis of rotation. Angular velocity $\Omega$ is the rotation rate of the dish. See text for further explanation.

*Continued on next page*

[3] The time interval between successive transits of a star over a meridian.

*7.1 Continued*

period $2\pi/\Omega$, which exactly matches the period of rotation of the dish. The shape and orientation of these trajectories will depend on the initial position and velocity of the marble. In this example, the marble is released at radius $r = r_0$ with no initial velocity. After the marble is released it rolls back and forth, like the tip of a pendulum, along the straight line pictured in Fig. 7.7, with a period equal to $2\pi/\Omega$, the same as the period of rotation of the dish. This oscillatory solution is represented by the equation

$$r = r_0 \cos \Omega t$$

where $t$ is time and radius $r$ is defined as positive on the side of the dish from which the marble is released and negative on the other side. The velocity of the marble along its pendulum-like trajectory

$$\frac{dr}{dt} = -\Omega r_0 \sin \Omega t$$

is largest at the times when it passes through the center of the dish at $t = \pi/2,\ 3\pi/2 \ldots$, and the marble is motionless for an instant at $t = \pi, 2\pi \ldots$ when it reverses direction at the outer edge of its trajectory.

In the rotating frame of reference the only force in the horizontal equation of motion is the Coriolis force, so the governing equation is

$$\frac{d\mathbf{c}}{dt} = -2\Omega\mathbf{k} \times \mathbf{c}$$

where $\mathbf{c}$ is the velocity of the marble and $\mathbf{k}$ is the vertical (normal to the surface of the dish) unit vector. Because $d\mathbf{c}/dt$ is perpendicular to $\mathbf{c}$, it follows that $c$, the speed of the marble as it moves along its trajectory in the rotating frame of reference, must be constant. The direction of the forward motion of the marble is changing with time at the uniform rate $2\Omega$, which is exactly twice the rate of rotation of the dish. Hence, the marble executes a circular orbit called an *inertia circle*, with period $2\pi/2\Omega = \pi/\Omega$ (i.e., half the period of rotation of the dish), with circumference $c\ (\pi/\Omega)$, and radius $c\ (\pi/\Omega)/2\pi = c/2\Omega$. Because $d\mathbf{c}/dt$ is to the right of $\mathbf{c}$, it follows that the marble rolls clockwise, i.e., in the opposite sense as the rotation of the dish.

As in the fixed frame of reference, the trajectory of the marble depends on its initial position and relative motion. Because the marble is released at radius $r_0$ with no initial motion in the fixed frame of reference, it follows that its speed in the rotating frame of reference is $c = \Omega r_0$, and thus the radius of the inertia circle is $\Omega r_0/2\Omega = r_0/2$. It follows that the marble passes through the center of the dish at the midpoint of its trajectory around the inertia circle.

The motion of the marble in the fixed and rotating frames of reference is shown in Fig. 7.8. The rotating dish is represented by the large circle. The point of release of the marble is labeled **0** and appears at the top of the diagram rather than on the left side of the dish as in Fig. 7.7. The pendulum-like trajectory of the marble in the fixed frame of reference is represented by the straight

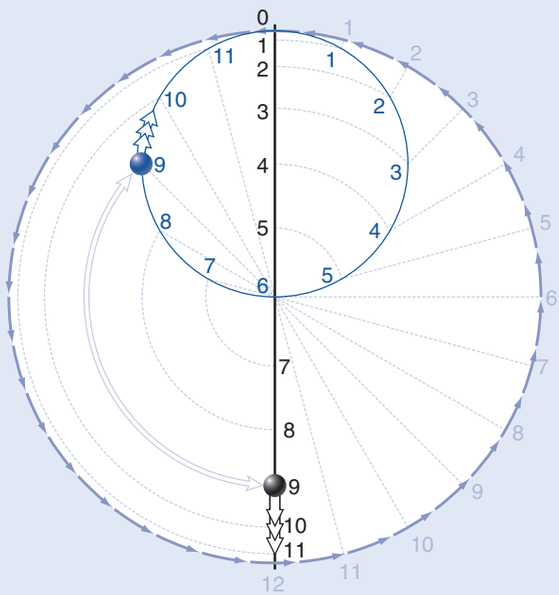


**Fig. 7.8** Trajectories of a frictionless marble in fixed (black) and rotating (blue) frames of reference. Numbered points correspond to positions of the marble at various times after it is released at point **0**. One complete rotation of the dish corresponds to one swing back and forth along the straight vertical black line in the fixed frame of reference and two complete circuits of the marble around the blue inertia circle in the rotating frame of reference. The light lines are reference lines. See text for further explanation.

*7.1 Continued*

black vertical line passing through the center of the dish. Successive positions along the trajectory at equally spaced time intervals are represented by numbers: point **1** represents the position of the marble after 1/24 of the period of rotation of the dish, point **12** after one-half period of rotation, etc. Hence, the numerical values assigned to the points are analogous to the 24 h of the day on a rotating planet. Note that the spacing between successive points is largest near the middle of the pendulum-like trajectory, where the marble is rolling fastest.

The position of the marble in the rotating (blue) frame of reference can be located at any specified time without invoking the Coriolis force simply by subtracting the displacement of the dish from the displacement of the marble in the fixed frame of reference. For example, to locate the marble after one-eighth rotation of the dish, we rotate point **3** clockwise (i.e., in the direction opposite to the rotation of the dish) one-eighth of the way around the circle; point **9** needs to be rotated three-eighths of the way around the circle, and so forth. The rotated points map out the trajectory of the marble in the rotating frame of reference: an inertia circle with a period equal to one-half revolution of the dish (i.e., 12 "hours"). In Fig. 7.8 the marble is pictured at 9 o'clock on the 24-hour clock in the two frames of reference.

Alternatively, the inertia circle can be constructed by first rotating the marble backward (clockwise) from its point of release to subtract the rotation of the dish and then moving the marble radially the appropriate distance along its pendulum-like trajectory. Reference lines for performing these operations are shown in Fig. 7.8. Examples of trajectories for two other sets of initial conditions are presented in Exercise 7.14.

### 7.2.2 Real Forces

The real forces that enter into the equations of motion are *gravity*, the *pressure gradient force*, and *frictional force* exerted by neighboring air parcels or adjacent surfaces.

#### *a. The pressure gradient force*

The vertical component of the pressure gradient force (per unit mass) $-(1/\rho)\partial p/\partial z$ has already been introduced in the context of the hydrostatic equation. The horizontal component of the pressure gradient force is given by the analogous expression

$$\mathbf{P} \equiv -\frac{1}{\rho}\nabla p \tag{7.8a}$$

or, in component form,

$$P_x = -\frac{1}{\rho}\frac{\partial p}{\partial x}; \quad P_y = -\frac{1}{\rho}\frac{\partial p}{\partial y} \tag{7.8b}$$

The pressure gradient force is directed down the horizontal pressure gradient $\nabla p$ from higher toward lower pressure. Making use of the hydrostatic equation (3.17) and the definitions of geopotential (3.20) and geopotential height (3.22), the horizontal pressure gradient force can be expressed in the alternative forms

$$\mathbf{P} \equiv -g\nabla z = -g_0\nabla Z = -\nabla\Phi \tag{7.9}$$

where the gradients of geometric height, geopotential height, and geopotential are defined on sloping pressure surfaces. Hence, the pressure gradient force can be interpreted as the component of effective gravity $g$ in the plane of the pressure surface, analogous to the "downhill" force on a ball rolling on a sloping surface. Pressure surfaces exhibit typical slopes on the order of 100 m per thousand kilometers, or 1 in $10^4$. Hence, the horizontal component of the pressure gradient force is roughly four orders of magnitude smaller than the vertical component; i.e., it is on the order of $10^{-3}$ m s$^{-2}$.

The pressure field on weather charts is typically represented by a set of contours plotted at regularly spaced intervals as in Fig. 1.19. The lines that are used to depict the distribution of pressure on geopotential height surfaces are referred to as *isobars*, and the lines used to depict the distribution of geopotential height on pressure surfaces are referred to as *geopotential height contours*. Exercise 3.4 demonstrates that, to a close approximation, isobars on a constant geopotential surface (e.g., sea level) can be converted into geopotential height contours on a

nearby pressure surface simply by relabeling them using a constant of proportionality based on the hypsometric equation (3.29). For example, near sea level, where atmospheric pressure decreases with height at a rate of ~1 hPa per 8 m, the conventional 4-hPa contour interval for isobars of sea-level pressure is approximately equivalent to a 30-m contour interval for geopotential height contours on a specified pressure surface. It follows that (7.8) and (7.9) yield virtually identical distributions of **P**.

In the oceans the horizontal pressure gradient force is due to both the gradient in sea level on a surface of constant geopotential and horizontal gradients in the ~~density~~ of the overlying water in the column. Near the ocean surface this force is primarily associated with the horizontal gradient in sea level. The topography of sea level is difficult to estimate in an absolute sense from observations because Earth's *geoid* (i.e., geopotential field) exhibits nonellipsoidal irregularities of its own that have more to do with plate tectonics than with oceanography. Temporal variations in sea level relative to Earth's much more slowly evolving geoid are clearly revealed by satellite altimetry.

### *b. The frictional force*

The frictional force (per unit mass) is given by

$$\mathbf{F} = -\frac{\partial \tau}{\partial z} \tag{7.10}$$

where $\tau$ represents the vertical component of the *shear stress* (i.e., the rate of vertical exchange of horizontal momentum) in units of N m$^{-2}$ due to the presence of smaller, unresolved scales of motion.[4] Vertical exchanges of momentum usually act to smooth out the vertical profile of **V**. The rate of vertical mixing that is occurring at any particular level and time depends on the strength of the vertical wind shear $\partial \mathbf{V}/\partial z$ and on the intensity of the unresolved motions, as discussed in Chapter 9. In the free atmosphere, above the boundary layer, the frictional force is much smaller than the pressure gradient force and the Coriolis force. However, within the boundary layer the frictional force is comparable in magnitude to the other terms in the horizontal equation of motion and needs to be taken into account.

The shear stress $\tau_s$ at the Earth's surface is in the opposing direction to the surface wind vector $\mathbf{V}_s$ (i.e., it is a "drag" on the surface wind) and can be approximated by the empirical relationship

$$\tau_s = -\rho C_D \mathbf{V}_s V_s \tag{7.11}$$

where $\rho$ is the density of the air, $C_D$ is a dimensionless *drag coefficient*, the magnitude of which varies with the roughness of the underlying surface and the static stability, $\mathbf{V}_s$ is the surface wind vector, and $V_s$ is the (scalar) surface wind speed. Within the lowest few tens of meters of the atmosphere, the stress decreases with height without much change in direction. Hence, within this so-called *surface layer*, the frictional force $\mathbf{F}_s = -\partial\tau/\partial z$ is directed opposite to $\mathbf{V}_s$ and is referred to as *frictional drag*.

## 7.2.3 The Horizontal Equation of Motion

The horizontal component of (7.6), written in vectorial form, per unit mass, is

$$\frac{d\mathbf{V}}{dt} = \mathbf{P} + \mathbf{C} + \mathbf{F} \tag{7.12}$$

where $d\mathbf{V}/dt$ is the Lagrangian time derivative of the horizontal velocity component experienced by an air parcel as it moves about in the atmosphere. Substituting for **C** from (7.7) and for **P** from (7.8a) we obtain

$$\frac{d\mathbf{V}}{dt} = -\frac{1}{\rho}\nabla p - f\mathbf{k} \times \mathbf{V} + \mathbf{F} \tag{7.13a}$$

or, in component form,

$$\frac{du}{dt} = -\frac{1}{\rho}\frac{\partial p}{\partial x} + fv + F_x,$$

$$\frac{dv}{dt} = -\frac{1}{\rho}\frac{\partial p}{\partial y} - fu + F_y \tag{7.13b}$$

The density dependence can be eliminated by substituting for **P** using (7.9) instead of (7.8), which yields

$$\frac{d\mathbf{V}}{dt} = -\nabla\Phi - f\mathbf{k} \times \mathbf{V} + \mathbf{F} \tag{7.14}$$

[4] The contributions of the corresponding horizontal exchanges of momentum to **F** do not need to be considered because the horizontal gradients are much smaller than the vertical gradients.

In (7.13a) the horizontal wind field is defined on surfaces of constant geopotential so that $\nabla\Phi = 0$, whereas in (7.14) it is defined on constant pressure surfaces so that $\nabla p = 0$. However, pressure surfaces are sufficiently flat that the **V** fields on a geopotential surface and a nearby pressure surface are very similar.

### 7.2.4 The Geostrophic Wind

In large-scale wind systems such as baroclinic waves and extratropical cyclones, typical horizontal velocities are on the order of $10\ \mathrm{m\ s^{-1}}$ and the timescale over which individual air parcels experience significant changes in velocity is on the order of a day or so ($\sim 10^5$ s). Thus a typical parcel acceleration $d\mathbf{V}/dt$ is $\sim 10\ \mathrm{m\ s^{-1}}$ per $10^5$ s or $10^{-4}\ \mathrm{m\ s^{-2}}$. In middle latitudes, where $f \sim 10^{-4}\ \mathrm{s^{-1}}$, an air parcel moving at a speed of $10\ \mathrm{m\ s^{-1}}$ experiences a Coriolis force per unit mass $\mathbf{C} \sim 10^{-3}\ \mathrm{m\ s^{-2}}$, about an order of magnitude larger than the typical horizontal accelerations of air parcels.

In the free atmosphere, where the frictional force is usually very small, the only term that is capable of balancing the Coriolis force **C** is the pressure gradient force **P**. Thus, to within about 10%, in middle and high latitudes, the horizontal equation of motion (7.14) is closely approximated by

$$f\mathbf{k} \times \mathbf{V} \simeq -\nabla\Phi$$

Making use of the vector identity

$$\mathbf{k} \times (\mathbf{k} \times \mathbf{V}) = -\mathbf{V}$$

it follows that

$$\mathbf{V} \simeq \frac{1}{f}(\mathbf{k} \times \nabla\Phi)$$

For any given horizontal distribution of pressure on geopotential surfaces (or geopotential height on pressure surfaces) it is possible to define a *geostrophic*[5] *wind field* $\mathbf{V}_g$ for which this relationship is exactly satisfied:

$$\mathbf{V}_g \equiv \frac{1}{f}(\mathbf{k} \times \nabla\Phi) \tag{7.15a}$$

or, in component form,

$$u_g = -\frac{1}{f}\frac{\partial\Phi}{\partial y}, \quad v_g = \frac{1}{f}\frac{\partial\Phi}{\partial x} \tag{7.15b}$$

or, in natural coordinates,

$$V_g \equiv \frac{1}{f}\frac{\partial\Phi}{\partial n} \tag{7.15c}$$

where $V_g$ is the scalar geostrophic wind speed and $n$ is the direction normal to the isobars (or geopotential height contours), pointing toward higher values.

The balance of horizontal forces implicit in the definition of the geostrophic wind (for a location in the northern hemisphere) is illustrated in Fig. 7.9. In order for the Coriolis force and the pressure gradient force to balance, the geostrophic wind must blow parallel to the isobars, leaving low pressure to the left. In either hemisphere, the geostrophic wind field circulates cyclonically around a center of low pressure and vice versa, as in Fig. 1.14, justifying the identification of local pressure minima with cyclones and local pressure maxima with anticyclones. The tighter the spacing of the isobars or geopotential height contours, the stronger the Coriolis force required to balance the pressure gradient force and hence, the higher the speed of the geostrophic wind.

### 7.2.5 The Effect of Friction

The three-way balance of forces required for flow in which $d\mathbf{V}/dt = 0$ in the northern hemisphere in the presence of friction at the Earth's surface is illustrated in Fig. 7.10. As in Fig. 7.9, **P** is directed normal

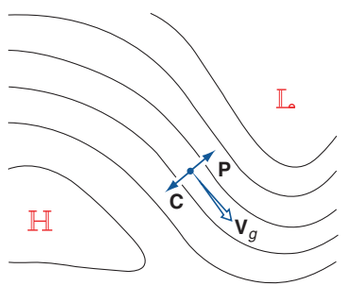


**Fig. 7.9** The geostrophic wind $V_g$ and its relationship to the horizontal pressure gradient force P and the Coriolis force C.

[5] >From the Greek: *geo* (Earth) and *strephen* (to turn)

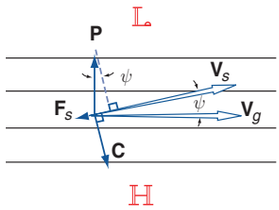


**Fig. 7.10** The three-way balance of forces required for steady surface winds in the presence of the frictional drag force F in the northern hemisphere. Solid lines represent isobars or geopotential height contours on a weather chart.

to the isobars, **C** is directed to the right of the horizontal velocity vector $\mathbf{V}_s$, and, consistent with (7.11), $\mathbf{F}_s$ is directed opposite to $\mathbf{V}_s$. The angle $\psi$ between $\mathbf{V}_s$ and $\mathbf{V}_g$ is determined by the requirement that the component of **P** in the forward direction of $\mathbf{V}_s$ must be equal to the magnitude of the drag $\mathbf{F}_s$, and the wind speed $V_s$ is determined by the requirement that **C** be just large enough to balance the component of **P** in the direction normal to $\mathbf{V}_s$; i.e.,

$$fV_s = |\mathbf{P}| \cos \psi$$

It follows that $|\mathbf{C}| < |\mathbf{P}|$ and, hence, the scalar wind speed $V_s = |\mathbf{C}|/f$ must be smaller than $V_g = |\mathbf{P}|/f$. The stronger the frictional drag force $\mathbf{F}_s$, the larger the angle $\psi$ between $\mathbf{V}_g$ and $\mathbf{V}_s$ and the more *subgeostrophic* the surface wind speed $\mathbf{V}_s$. The cross-isobar flow toward lower pressure, referred to as the *Ekman*[6] *drift*, is clearly evident on surface charts, particularly over rough land surfaces. That the winds usually blow nearly parallel to the isobars in the free atmosphere indicates that the significance of the frictional drag force is largely restricted to the boundary layer, where small-scale turbulent motions are present.

The same shear stress that acts as a drag force on the surface winds exerts a forward pull on the surface waters of the ocean, giving rise to *wind-driven currents*. Away from the coastlines and the equator, the frictional force averaged over the topmost few tens of meters is much stronger than the pressure gradient force associated with the sloping sea level. In these regions the balance of forces in the uppermost few meters of the ocean is characterized by a two-way balance between the forward pull of the surface wind and the backward pull of the Coriolis force, as shown in Fig. 7.11. The surface currents and horizontal mass transport are thus dominated by the Ekman drift, which is directed toward the right of the surface wind vector in the northern hemisphere and to the left of the surface wind vector in the southern hemisphere. Polar sea ice behaves in a similar manner. With increasing depth below the ocean surface, the frictional force declines in importance relative to the horizontal pressure gradient force and the flow progressively becomes more geostrophic. Below a depth of ~50 m the flow in the ocean is predominantly geostrophic.

The turning of the ocean currents with depth as one progresses downward from the frictionally dominated regime in the topmost few tens of meters to the geostrophic regime below is referred to as the *Ekman spiral*. The wind in the atmospheric boundary layer exhibits a more subtle Ekman spiral, turning with height from $\mathbf{V}_s$ at the Earth's surface to $\mathbf{V}_g$ at the top of the boundary layer.

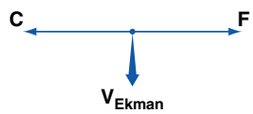


**Fig. 7.11** The force balance associated with Ekman drift in the northern hemisphere oceans. The frictional force F is in the direction of the surface wind vector. In the southern hemisphere (not shown) the Ekman drift is to the left of the surface wind vector.

[6] **V. Walfrid Ekman** (1874–1954) Swedish oceanographer. Ekman was introduced to the problem of wind-driven ocean circulation when he was a student working under the direction of Professor Vilhelm Bjerknes.[7] Fridtjof Nansen had approached Bjerknes with a remarkable set of observations of winds and ice motions taken during the voyage of the *Fram*, for which he sought an explanation. Nansen's observations and Ekman's mathematical analysis are the foundations of the theory of the wind-driven ocean circulation.

[7] **Vilhelm Bjerknes** (1862–1951). Norwegian physicist and one of the founders of the science of meteorology. Held academic positions at the universities of Stockholm, Bergen, Leipzig, and Kristiania (renamed Oslo). Proposed in 1904 that weather prediction be regarded as an initial value problem that could be solved by integrating the governing equations forward in time, starting from an initial state determined by current weather observations. Best known for his work at Bergen (1917–1926) where he assembled a small group of dedicated and talented young researchers, including his son Jacob. The most widely recognized achievement of this so-called "Bergen School" was a conceptual framework for interpreting the structure and evolution of extratropical cyclones and fronts that has endured until the present day.

### 7.2.6 The Gradient Wind

The centripetal accelerations observed in association with the curvature of the trajectories of air parcels tend to be much larger than those associated with the speeding up or slowing down of air parcels as they move downstream. Hence, when $d\mathbf{V}/dt$ is large, its scalar magnitude can be approximated by the centripetal acceleration $V^2/R_T$, where $R_T$ is the local radius of curvature of the air trajectories.[8] Hence, the horizontal equation of motion reduces to the balance of forces in the direction transverse to the flow, i.e.,

$$\frac{V^2}{R_T} = -\nabla\Phi - f\mathbf{k} \times \mathbf{V} \tag{7.16}$$

The signs of the terms in this three-way balance depend on whether the curvature of the trajectories is cyclonic or anticyclonic, as illustrated in Fig. 7.12. In the cyclonic case, the outward centrifugal force (the mirror image of the centripetal acceleration) reinforces the Coriolis force so that a balance can be achieved with a wind speed smaller than would be required if the Coriolis force were acting alone. In flow through sharp troughs, where the curvature of the trajectories is cyclonic, the observed wind speeds at the jet stream level are often smaller, by a factor of two or more, than the geostrophic wind speed implied by the spacing of the isobars. For the anticyclonically curved trajectory on the right in Fig. 7.12 the centrifugal force opposes the Coriolis force, necessitating a *supergeostrophic* wind speed in order to achieve a balance.

The wind associated with a three-way balance between the pressure gradient and Coriolis and centrifugal forces is called the *gradient wind*. The solution of (7.16), which yields the speed of the gradient wind can be written in the form

$$V_{gr} = \frac{1}{f}\left(|\nabla\Phi| + \frac{V_{gr}^2}{R_T}\right) \tag{7.17}$$

and solved using the quadratic formula. From Fig. 7.12, it can be inferred that $R_T$ should be specified as positive if the curvature is cyclonic and negative if the curvature is anticyclonic. For the case of anticyclonic curvature, a solution exists when

$$|\nabla\Phi| < fV - \frac{V^2}{R_T}$$

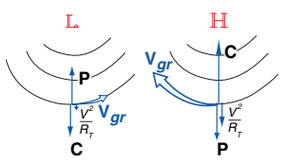


**Fig. 7.12** The three-way balance involving the horizontal pressure gradient force P, the Coriolis force C, and the centrifugal force $|V|^2/R_T$ in flow along curved trajectories in the northern hemisphere. (Left) Cyclonic flow. (Right) Anticyclonic flow.

### 7.2.7 The Thermal Wind

Just as the geostrophic wind bears a simple relationship to $\nabla\Phi$, the vertical shear of the geostrophic wind bears a simple relationship to $\nabla T$. Writing the geostrophic equation (7.14) for two different pressure surfaces and subtracting, we obtain an expression for the vertical wind shear in the intervening layer

$$(\mathbf{V}_g)_2 - (\mathbf{V}_g)_1 = -\frac{1}{f}\mathbf{k} \times \nabla(\Phi_2 - \Phi_1) \tag{7.18}$$

In terms of geopotential height

$$(\mathbf{V}_g)_2 - (\mathbf{V}_g)_1 = -\frac{g_0}{f}\mathbf{k} \times \nabla(Z_2 - Z_1) \tag{7.19a}$$

or. in component form,

$$(u_g)_2 - (u_g)_1 = -\frac{g_0}{f}\frac{\partial Z}{\partial y},$$
$$(v_g)_2 - (v_g)_1 = \frac{g_0}{f}\frac{\partial Z}{\partial x} \tag{7.19b}$$

This expression, known as the *thermal wind equation*, states that the vertically averaged vertical shear of the geostrophic wind within the layer between any two pressure surfaces is related to the horizontal gradient of thickness of the layer in the same manner in which geostrophic wind is related to geopotential height. For example, in the northern hemisphere

[8] In estimating the radius of curvature in the gradient wind equation it is important to keep in mind the distinction between *streamlines* and *trajectories*, as explained in Section 8.1.4.

the *thermal wind* (namely the vertical shear of the geostrophic wind) "blows" parallel to the thickness contours, leaving low thickness to the left. Incorporating the linear proportionality between temperature and thickness in the hypsometric equation (3.29), the thermal wind equation can also be expressed as a linear relationship between the vertical shear of the geostrophic wind and the horizontal temperature gradient.

$$(\mathbf{V}_g)_2 - (\mathbf{V}_g)_1 = -\left(\frac{R}{f}\ln\frac{p_1}{p_2}\right)\mathbf{k}\times\nabla(\overline{T}) \qquad (7.20)$$

where $\overline{T}$ is the vertically averaged temperature within the layer.

To explore the implications of the thermal wind equation, consider first the special case of an atmosphere that is characterized by a total absence of horizontal temperature (thickness) gradients. In such a *barotropic*[9] atmosphere $\nabla T = 0$ on constant pressure surfaces. Because the thickness of the layer between any pair of pressure surfaces is horizontally uniform, it follows that the geopotential height contours on various pressure surfaces can be neatly stacked on top of one another, like a set of matched dinner plates. It follows that the direction and speed of the geostrophic wind must be independent of height.

Now let us consider an atmosphere with horizontal temperature gradients subject to the constraint that the thickness contours be everywhere parallel to the geopotential height contours. For historical reasons, such a flow configuration is referred to as *equivalent barotropic*. It follows from the thermal wind equation that the vertical wind shear in an equivalent barotropic atmosphere must be parallel to the wind itself so the direction of the geostrophic wind does not change with height, just as in the case of a pure barotropic atmosphere. However, the slope of the pressure surfaces and hence the speed of the geostrophic wind may vary from level to level in association with thickness variations in the direction normal to height contours, as illustrated in Fig. 7.13.

In an equivalent barotropic atmosphere, the isobars and isotherms on horizontal maps have the same shape. If the highs are warm and the lows are cold, the amplitude of features in the pressure field pressure and the speed of the geostrophic wind

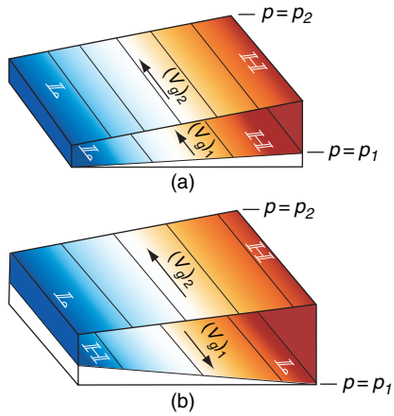


**Fig. 7.13** The change of the geostrophic wind with height in an equivalent barotropic flow in the northern hemisphere: (a) $V_g$ increasing with height within the layer and (b) $V_g$ reversing direction. The temperature gradient within the layer is indicated by the shading: blue (cold) coincides with low thickness and tan (warm) with high thickness.

increase with height. If the highs are cold and the lows are warm, the situation is just the opposite; features in the pressure and geostrophic wind field tend to weaken with height and the wind may even reverse direction if the temperature anomalies extend through a deep enough layer, as in Fig. 7.13b. The zonally averaged zonal wind and temperature cross sections shown in Fig. 1.11 are related in a manner consistent with Fig. 7.13. Wherever temperature decreases with increasing latitude, the zonal wind becomes (relatively) more westerly with increasing height, and vice versa.

***Exercise 7.3*** During winter in the troposphere ~30° latitude, the zonally averaged temperature gradient is ~0.75 K per degree of latitude (see Fig. 1.11) and the zonally averaged component of the geostrophic wind at the Earth's surface is close to zero. Estimate the mean zonal wind at the jet stream level, ~250 hPa.

***Solution:*** Taking the zonal component of (7.20) and averaging around a latitude circle yields

$$[u_g]_{250} - [u_g]_{1000} = -\frac{R}{2\Omega\sin\phi}\frac{\partial[T]}{\partial y}\ln\frac{1000}{250}$$

[9] The term barotropic is derived from the Greek *baro*, relating to pressure, and *tropic*, changing in a specific manner: that is, in such a way that surfaces of constant pressure are coincident with surfaces of constant temperature or density.

Noting that $[u_g]_{1000} \simeq 0$ and $R \simeq R_d$

$$[u_g]_{250} = -\frac{287 \text{ J deg}^{-1} \text{ kg}^{-1}}{2 \times 7.29 \times 10^{-5} \text{ s}^{-1} \sin 30^\circ} \times \ln 4 \times \frac{-0.75 \text{ K}}{1.11 \times 10^5 \text{ m}} = 36.8 \text{ m s}^{-1},$$

in close agreement with Fig. 1.11. ■

In a fully *baroclinic atmosphere*, the height and thickness contours intersect one another so that the geostrophic wind exhibits a component normal to the isotherms (or thickness contours). This geostrophic flow across the isotherms is associated with *geostrophic temperature advection. Cold advection* denotes flow across the isotherms from a colder to a warmer region, and vice versa.

Typical situations corresponding to cold and warm advection in the northern hemisphere are illustrated in Fig. 7.14. On the pressure level at the bottom of the layer the geostrophic wind is from the west so the height contours are oriented from west to east, with lower heights toward the north. Higher thickness lies toward the east in the cold advection case (Fig. 7.14a) and toward the west in the warm advection case (Fig. 7.14b).[10]

The upper level geostrophic wind vector $\mathbf{V}_{g2}$ blows parallel to these upper-level contours. Just as the upper level geopotential height is the algebraic sum of the lower level geopotential height $Z_1$ plus the thickness $Z_T$, the upper level geostrophic wind vector $\mathbf{V}_{g2}$ is the vectorial sum of the lower level geostrophic wind $\mathbf{V}_{g1}$ plus the thermal wind $\mathbf{V}_T$. Hence, *thermal wind* is to *thickness* as *geostrophic wind* is to *geopotential height*.

>From Fig. 7.14 it is apparent that cold advection is characterized by *backing* (cyclonic rotation) of the geostrophic wind vector with height and warm advection is characterized by *veering* (anticyclonic rotation). By experimenting with other configurations of height and thickness contours, it is readily verified that this relationship holds, regardless of the direction of the geostrophic wind at the bottom of the layer or the orientation of the isotherms, and it holds for the southern hemisphere as well.

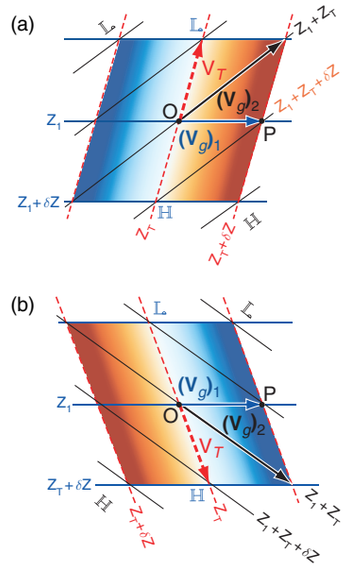


**Fig. 7.14** Relationships among isotherms, geopotential height contours, and geostrophic wind in layers with (a) cold and (b) warm advection. Solid blue lines denote the geopotential height contours at the bottom of the layer and solid black lines denote the geopotential height contours at the top of the layer. Red lines represent the isotherms or thickness contours within the layer.

Making use of the thermal wind equation it is possible to completely define the geostrophic wind field on the basis of knowledge of the distribution of $T(x, y, p)$, together with boundary conditions for either $p(x, y)$ or $\mathbf{V}_g(x, y)$ at the Earth's surface or at some other "reference level." Thus, for example, a set of sea level pressure observations together with an array of closely spaced temperature soundings from satellite-borne sensors constitutes an observing system suitable for determining the three-dimensional distribution of $\mathbf{V}_g$.

[10] Given the distribution of geopotential height $Z_1$ at the lower level and thickness $Z_T$, it is possible to infer the geopotential height $Z_2$ at the upper level by simple addition. For example, the height $Z_2$ at point O at the center of the diagram is equal to $Z_1 + Z_T$, and at point P it is $Z_1 + (Z_T + \Delta Z)$, and so forth. The upper-level height contours (solid black lines) are drawn by connecting intersections with equal values of this sum. If the fields of $Z_1$, $Z_2$, and $Z_T$ are all displayed using the same contour interval (say, 60 m), then all intersections between countours will be three-way intersections. In a similar manner, given a knowledge of the geopotential height field at the lower and upper levels, it is possible to infer the thickness field $Z_T$ by subtracting $Z_1$ from $Z_2$.

### 7.2.8 Suppression of Vertical Motions by Planetary Rotation[11]

Through the action of the Coriolis force, Earth's rotation imparts a special character to large-scale motions in the atmosphere and oceans. In the absence of planetary rotation, typical magnitudes of the horizontal and vertical motion components (denoted here as $U$ and $W$, respectively) would scale, relative to one another, in proportion to their respective length ($L$) and depth scales ($D$) of the horizontal and vertical motions, i.e.,

$$\frac{W}{U} \sim \frac{D}{L}$$

Boundary layer turbulence and convection, whose timescales are much shorter then the planetary rotation do, in fact, scale in such a manner. However, the vertical component of large-scale motions is smaller than would be expected on the basis of their aspect ratio. For example, in extratropical latitudes the depth scale is $\sim$5 km (half the depth of the troposphere) and the length scale is $\sim$1000 km: hence, $D/L \sim 1/200$. Typical horizontal velocities in these systems are $\sim 10\ \mathrm{m\ s^{-1}}$. The corresponding vertical velocities, scaled in accordance with a 1/200 aspect ratio, should be $\sim 5\ \mathrm{cm\ s^{-1}}$. However, the observed vertical velocities ($\sim 1\ \mathrm{cm\ s^{-1}}$) are almost an order of magnitude smaller than that.

Similar considerations apply to the ratio of typical values of divergence and vorticity observed in large-scale horizontal motions. Because these quantities involve horizontal derivatives of the horizontal wind field, one might expect them both to scale as

$$\frac{U}{L} \sim \frac{10\ \mathrm{m\ s^{-1}}}{1{,}000\ \mathrm{km}} = \frac{10\ \mathrm{m\ s^{-1}}}{10^6\ \mathrm{m}} = 10^{-5}\ \mathrm{s^{-1}}$$

just like the elementary properties of the horizontal flow (shear, curvature, diffluence and stretching) and the terms $\partial u/\partial x$, $\partial u/\partial y$, $\partial v/\partial x$, and $\partial v/\partial y$ in Cartesian coordinates. Vorticity does, in fact, scale in such a manner, but typical values of the divergence are $\sim 10^{-6}\ \mathrm{s^{-1}}$, almost an order of magnitude smaller than $U/L$.

The smallness of the divergence in a rotating atmosphere reflects a high degree of compensation between diffluence and stretching terms, with diffluence occurring in regions in which the flow is slowing down as it moves downstream, and vice versa. This *quasi-nondivergent* character of the horizontal wind field is in sharp contrast to the flow of motor vehicles on a multilane highway, in which a narrowing of the roadway is marked by a slowdown of traffic. A similar compensation is observed between the terms in the Cartesian form of the divergence; that is, to within 10–20%

$$\frac{\partial u}{\partial x} \sim -\frac{\partial v}{\partial y}$$

Because estimates of the divergence require estimating a small difference between large terms, they tend to be highly sensitive to errors in the wind field. The geostrophic wind field also tends to be quasi-nondivergent, but not completely so, because of the variation of the Coriolis parameter $f$ with latitude (see Exercise 7.20).

### 7.2.9 A Conservation Law for Vorticity

A major breakthrough in the development of modern atmospheric dynamics was the realization, in the late 1930s, that many aspects of the behavior of large-scale extratropical wind systems can be understood on the basis of variants of a single equation based on the conservation of vorticity of the horizontal wind field.[12] To a close approximation, the time rate of change of vorticity can be written in the form

$$\frac{\partial}{\partial t}(f + \zeta) = -\mathbf{V} \cdot \nabla(f + \zeta) - (f + \zeta)(\nabla \cdot \mathbf{V}) \quad (7.21a)$$

or, in Lagrangian form,

$$\frac{d}{dt}(f + \zeta) = -(f + \zeta)(\nabla \cdot \mathbf{V}) \quad (7.21b)$$

In these expressions, $\zeta$, the vorticity of the horizontal wind field, appears in combination with the Coriolis

[11] The remainder of this section introduces the student to more advanced dynamical concepts that are not essential for an understanding of subsequent sections of this chapter. For a more thorough and rigorous treatment of this material, see J. R. Holton, *Introduction to Dynamical Meteorology*, Fourth edition, Academic Press (2004).

[12] We offer a proof of this so-called *vorticity equation* in Exercise 7.32.

parameter $f$, which can be interpreted as the *planetary vorticity* that exists by virtue of the Earth's rotation: $2\Omega$ (as inferred from Exercise 7.1) times the cosine of the angle between the Earth's axis of rotation and the local vertical (i.e., the colatitude). Hence, $(f + \zeta)$ is the *absolute vorticity*: the sum of the *planetary vorticity* and the *relative vorticity* of the horizontal wind field. In extratropical latitudes, where $f \sim 10^{-4}\ s^{-1}$ and $\zeta \sim 10^{-5}\ s^{-1}$, the absolute vorticity is dominated by the planetary vorticity. In tropical motions the relative and planetary vorticity terms are of comparable magnitude.

In fast-moving extratropical weather systems that are not rapidly amplifying or decaying, the divergence term in (7.21) is relatively small so that

$$\frac{\partial \zeta}{\partial t} \simeq -\mathbf{V} \cdot \nabla(\zeta + f) \tag{7.22a}$$

or, in Lagrangian form,

$$\frac{d}{dt}(\zeta + f) \simeq 0 \tag{7.22b}$$

In this simplified form of the vorticity equation, absolute vorticity $(\zeta + f)$ behaves as a *conservative tracer*: i.e., a property whose numerical values are conserved by air parcels as they move along with (i.e., are advected by) the horizontal wind field.

This nondivergent form of the vorticity equation was used as a basis for the earliest quantitative weather prediction models that date back to World War II.[13] The forecasts, which were based on the 500-hPa geopotential height field, involved a four-step process:

1. The *geostrophic vorticity*

$$\zeta_g \equiv \frac{\partial v_g}{\partial x} - \frac{\partial u_g}{\partial y} = \frac{1}{f}\left(\frac{\partial^2 \Phi}{\partial x^2} + \frac{\partial^2 \Phi}{\partial y^2}\right) \tag{7.23}$$

   is calculated for an array of grid points, using a simple finite difference algorithm,[14] and added to $f$ to obtain the absolute vorticity.
2. The advection term in (7.22a) is estimated to obtain the geostrophic vorticity tendency $\partial \zeta_g / \partial t$ at each grid point.
3. The corresponding geopotential height tendency $\chi \equiv \partial \Phi / \partial t$ at each grid-point is found by inverting and solving (7.23).
4. The $\chi$ field is multiplied by a small time step $\Delta t$ to obtain the incremental height change at each grid point and this change is added to the initial 500-hPa height field to obtain the forecast of the 500-hPa height field.

Let us consider the implications of applying this forecast model to an idealized geostrophic wind pattern with a sinusoidal wave with zonal wavelength $L$ superimposed on a uniform westerly flow with velocity $U$. The geostrophic vorticity $\zeta_g$ is positive in the wave troughs where the curvature of the flow is cyclonic, zero at the inflection points where the flow is straight, and negative in the ridges where the curvature is anticyclonic. The vorticity perturbations associated with the waves tend to be advected eastward by the westerly background flow: positive vorticity tendencies prevail in the southerly flow near the inflection points downstream of the troughs of the waves, and negative tendencies in the northerly flow downstream of the ridges (points A and B, respectively, in Fig. 7.15). The positive vorticity tendencies downstream of the troughs induce height falls, causing the troughs to propagate eastward, and similarly for the ridges. Were it not for the advection of planetary vorticity, the wave would propagate eastward at exactly the same speed as the "steering flow" $U$.

In addition to the vorticity tendency resulting from the advection of relative vorticity $\zeta$, equatorward flow induces a cyclonic vorticity tendency, as air from higher latitudes with higher planetary vorticity is

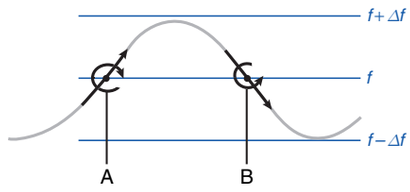


**Fig. 7.15** Patterns of vorticity ~~advection~~ induced by the horizontal advection of absolute vorticity in a wavy westerly flow in the northern hemisphere.

[13] The barotropic model was originally implemented with graphical techniques using a light table to overlay various fields. Later it was programmed on the first primitive computers.

[14] See J. R. Holton, *An Introduction to Dynamic Meteorology*, Academic Press, p. 452–453 (2004).

advected southward. Because absolute vorticity ($f + \zeta$) is conserved, the planetary vorticity of southward moving air parcels is, in effect, being converted to relative vorticity, inducing a positive tendency. In a similar manner, advection of low planetary vorticity by the poleward flow induces an anticyclonic vorticity tendency. In this manner the meridional gradient of planetary vorticity on a spherical Earth causes waves to propagate westward relative to the steering flow.

The relative importance of the tendencies induced by the advection of relative vorticity and planetary vorticity depends on the strength of the steering flow $U$ and on the zonal wavelength $L$ of the waves: other things being equal, the smaller the scale of the waves, the stronger the $\zeta$ perturbations, and hence the stronger the advection of relative vorticity. For baroclinic waves with zonal wavelengths ~4000 km, the advection of relative vorticity is much stronger than the advection of planetary vorticity and the influence of the advection of planetary vorticity is barely discernible. However, for *planetary waves* with wavelengths roughly comparable to the radius of the Earth, the much weaker eastward advection of relative vorticity is almost entirely cancelled by the advection of planetary vorticity so that the net vorticity tendencies in (7.24) are quite small. Waves with horizontal scales in this range tend to be quasi-stationary in the presence of the climatological-mean westerly steering flow. The monthly, seasonal, and climatological-mean maps discussed in Chapter 10 tend to be dominated by these so-called *stationary waves*.

The barotropic vorticity equation (7.22a) can be written in the form

$$\frac{\partial \zeta}{\partial t} \simeq -\mathbf{V} \cdot \nabla \zeta - \beta v \tag{7.24}$$

where

$$\beta \equiv \frac{\partial f}{\partial y} = \frac{\partial}{\partial y}\,(2\Omega \sin\phi) = \frac{2\Omega \cos\phi}{R_E} \tag{7.25}$$

In middle latitudes, $\beta \sim 10^{-11}\,\mathrm{s^{-1}\,m^{-1}}$. The term $-\beta v$ in (7.24) is commonly referred to as the *beta effect*. Wave motions in which the beta effect significantly influences the dynamics are referred to as *Rossby*[15] *waves*.

The divergence term in (7.21) is instrumental in the amplification of baroclinic waves, tropical cyclones, and other large-scale weather systems and in maintaining the vorticity perturbations in the low level wind field in the presence of frictional dissipation. In extratropical latitudes, where $f$ is an order of magnitude larger than typical values of $\zeta$, the divergence term is dominated by the linear term $-f\,(\nabla \cdot \mathbf{V})$, which represents the deflection of the cross-isobar flow by the Coriolis force. For example, the Coriolis force deflects air converging into a cyclone toward the right in the northern hemisphere (left in the southern hemisphere), producing (or intensifying) the cyclonic circulation about the center of the system. This term is capable of inducing vorticity tendencies on the order of

$$f(\nabla \cdot \mathbf{V}) \sim 10^{-4}\,\mathrm{s^{-1}} \times 10^{-6}\,\mathrm{s^{-1}} \sim 10^{-10}\,\mathrm{s^{-2}}$$

comparable to those induced by the vorticity advection term[16]

$$\mathbf{V} \cdot \nabla(\zeta) \sim 10\,\mathrm{m\,s^{-1}} \times \frac{10^{-5}\,\mathrm{s^{-1}}}{10^3\,\mathrm{km} \times 10^3\,\mathrm{m\,km^{-1}}}$$

$$\sim 10^{-10}\,\mathrm{s^{-2}}.$$

The nonlinear term $\zeta\,(\nabla \cdot \mathbf{V})$ in (7.21) also plays an important role in atmospheric dynamics. We can gain some insight into this term by considering the time-dependent solution of (7.21b), subject to the initial condition $\zeta = 0$ at $t = 0$, prescribing that $\nabla \cdot \mathbf{V} = C$, a constant. If the flow is divergent ($C > 0$), vorticity will initially decrease (become anticyclonic) at the rate $-fC$, but the rate of decrease will slow exponentially with time as $\zeta \to -f$ and $(f + \zeta) \to 0$. In contrast, if the flow is convergent ($C < 0$) the vorticity tendency

[15] **Carl Gustav Rossby** (1898–1957) Swedish meteorologist. Studied under Vilhelm Bjerknes, father of Jacob Bjerknes. Founded and chaired the Department of Meteorology at Massachusetts Institute of Techology and the Institute for Meteorology at the University of Stockholm. While serving as chair of the Department of Meteorology at the University of Chicago during World War II, he was instrumental in the training of meteorologists for the U.S. military, many of whom became leaders in the field.

[16] In the previous subsection the divergence term was assumed to be negligible in comparison to the horizontal advection term, whereas in this subsection it is treated as if it were comparable to it in magnitude. This apparent inconsistency is resolved in Section 7.3.4 when we consider the vertical structure of the divergence profile.

will be positive and will increase without limit as $\zeta$ grows.[17] This asymmetry in the rate of growth of relative vorticity perturbations is often invoked to explain why virtually all intense closed circulations are cyclones, rather than anticyclones, and why sharp frontal zones and shear lines nearly always exhibit cyclonic, rather than anticyclonic vorticity.

### 7.2.10 Potential Vorticity

It is possible to derive a conservation law analogous to (7.22) that takes into account the effect of the divergence of the horizontal motion. Consider a layer consisting of an incompressible fluid of depth $H(x, y)$ moving with velocity $\mathbf{V}(x, y)$. From the conservation of mass, we can write

$$\frac{d}{dt}(HA) = 0 \tag{7.26}$$

where $A$ is the area of an imaginary block of fluid, but it may also be interpreted as the area enclosed by a tagged set of fluid parcels as they move with the horizontal flow. Making use of (7.2), we can write

$$\frac{1}{H}\frac{dH}{dt} = -\frac{1}{A}\frac{dA}{dt} = -\nabla \cdot \mathbf{V}$$

Hence the layer thickens wherever the horizontal flow converges and thins where the flow diverges. Using this expression to substitute for the divergence in (7.21b) yields

$$\frac{d}{dt}(f + \zeta) = \frac{(f + \zeta)}{H}\frac{dH}{dt}$$

In Exercise 7.35 the student is invited to verify that this expression is equivalent to the simple conservation equation

$$\frac{d}{dt}\left(\frac{f + \zeta}{H}\right) = 0 \tag{7.27}$$

The conserved quantity in this expression is called the *barotropic potential vorticity*.

>From (7.27) it is apparent that vertical stretching of air columns and the associated convergence of the horizontal flow increase the absolute vorticity $(f + \zeta)$ in inverse proportion to the increase of $H$. The "spin up" of absolute vorticity that occurs when columns are vertically stretched and horizontally compressed is analogous to that experienced by an ice skater going into a spin by drawing his/her arms and legs inward as close as possible to the axis of rotation. The concept of potential vorticity also allows for conversions between relative and planetary vorticity, as described in the context of (7.22).

Based on an inspection of the form of (7.27) it is evident that a uniform horizontal gradient in the depth of a layer of fluid plays a role in vorticity dynamics analogous to the beta effect. Hence, Rossby waves can be defined more generally as waves propagating horizontally in the presence of a gradient of potential vorticity.

An analogous expression can be derived for the conservation of potential vorticity in large-scale, adiabatic atmospheric motions.[18] If the flow is adiabatic, air parcels cannot pass through isentropic surfaces (i.e., surfaces of constant potential temperature). It follows that the mass per unit area in the column bounded by two nearby isentropic surfaces is conserved following the flow; i.e.,

$$\frac{A\,\delta p}{g} = constant \tag{7.28}$$

where $\delta p$ is the pressure difference between two nearby isentropic surfaces separated by a fixed potential temperature increment $\delta\theta$, as depicted in Fig. 7.16. The pressure difference between the top

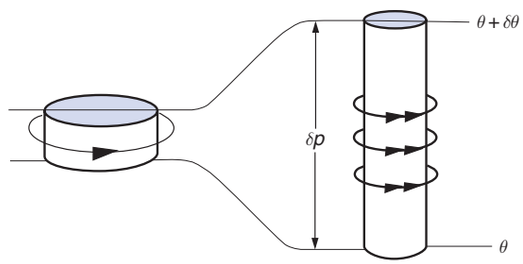


**Fig. 7.16** A cylindrical column of air moving adiabatically, conserving potential vorticity. [From J. R. Holton, *Introduction to Dynamic Meteorology*, 4th edition, Academic Press, p. 96 (2004)].

[17] Divergence tends to be inhibited by the presence of both planetary vorticity and relative vorticity. In this sense, prescribing the divergence to be constant while the relative vorticity is allowed to increase without limit is unrealistic.

[18] The conditions under which the assumption of adiabatic flow is justified are discussed in Section 7.3.3.

and the bottom of the layer is inversely proportional to the static stability, i.e.,

$$\delta_p = \left(\frac{\partial\theta}{\partial p}\right)^{-1}\delta\theta \tag{7.29}$$

The tighter the vertical spacing of the isentropes (i.e., the stronger the static stability), the smaller pressure increment (and mass per unit area) between the surfaces. Combining (7.28) and (7.29), absorbing $\delta\theta/g$ into the constant, and differentiating, following the large-scale flow, yields

$$\frac{d}{dt}\left[\left(\frac{\partial\theta}{\partial p}\right)^{-1}A\right] = 0 \tag{7.30}$$

Noting the analogy between (7.26) and (7.30) it follows that

$$\frac{d}{dt}\left[(f+\zeta_\theta)\frac{\partial\theta}{\partial p}\right] = 0 \tag{7.31a}$$

The conserved quantity in the square brackets is the isentropic form of *Ertel's*[19] *potential vorticity*, often referred to simply as *isentropic potential vorticity* (PV). The $\theta$ subscript in this expression specifies that the relative vorticity must be evaluated on potential temperature surfaces, rather than pressure surfaces. PV is conventionally expressed in units of *potential vorticity units* (PVU), which apply to the quantity in brackets in (7.31) multiplied by $g$, where 1 PVU = $10^{-6}$ m$^2$ s$^{-1}$ K kg$^{-1}$.

In synoptic charts and vertical cross sections, tropospheric and stratospheric air parcels are clearly distinguishable by virtue of their differing values of PV, with stratospheric air having higher values. The 1 PVU contour usually corresponds closely to the tropopause level. Poleward of westerly jet streams PV is enhanced by the presence of cyclonic wind shear, and in the troughs of waves it is enhanced by the cyclonic curvature of the streamlines. Hence the PV surfaces are depressed in these regions. Surfaces of constant ozone, water vapor, and other conservative chemical tracers are observed to dip downward in a similar manner, indicating a depression of the tropopause that conforms to the distortion of the PV surfaces. In a similar manner the PV surfaces and the tropopause itself are elevated on the equatorward flank of westerly jet streams, where the PV is relatively low due to the presence of anticyclonic wind shear, and in ridges and anticyclones, where the curvature of the flow is anticyclonic.

As air parcels move through various regions of the atmosphere it takes several days for their potential vorticity to adjust to the changing ambient conditions. Hence, incursions of stratospheric air into the troposphere are marked, not only by conspicuously low dew points and high ozone concentrations, but also by high values of potential vorticity, as manifested in high static stability $\partial\theta/\partial p$ and/or strong cyclonic shear or curvature.

The distribution of PV is uniquely determined by the wind and temperature fields. A prognostic equation analogous to (7.22a): namely, the Eulerian counterpart of (7.31a)

$$\frac{\partial}{\partial t}\left[(\zeta_\theta+f)\frac{\partial\theta}{\partial p}\right] = -\mathbf{V}_\theta\cdot\nabla\left[(\zeta_\theta+f)\frac{\partial\theta}{\partial p}\right] \tag{7.31b}$$

can be used to update PV field. The updated distribution of PV on potential temperature surfaces, together with the temperature distribution at the Earth's surface, can be inverted to obtain the updated three-dimensional distribution of wind and temperature. Although they are not as accurate as numerical weather prediction based on the primitive equations discussed in the next section, forecasts based on PV have provided valuable insights into the development of weather systems.

## 7.3 Primitive Equations

This section introduces the complete system of so-called *primitive equations*[20] that governs the evolution of large-scale atmospheric motions. The horizontal equation of motion (7.13) is a part of that system. The other primitive equations relate to the vertical component of the motion and to the time rates of change of the thermodynamic variables $p$, $\rho$, and $T$.

[19] **Hans Ertel** (1904–1971) German meteorologist and geophysicist. His theoretical studies, culminating in his potential vorticity theorem, were key elements in the development of modern dynamical meteorology.

[20] Here the term primitive connotes fundamental or basic; i.e., unrefined by scaling considerations other than the assumption of hydrostatic balance.

### 7.3.1 Pressure as a Vertical Coordinate

The primitive equations are easiest to explain and interpret when pressure, rather than geopotential height, is used as the vertical coordinate. The transformation from height $(x, y, z)$ to pressure $(x, y, p)$ coordinates is relatively straightforward because pressure and geopotential height are related through the hydrostatic equation (3.17) and surfaces of constant pressure are so flat we can ignore the distinction between the horizontal wind field $\mathbf{V}_p(x, y)$ on a surface of constant pressure and $\mathbf{V}_z(x, y)$ on a nearby surface of constant geopotential height.

The vertical velocity component in $(x, y, p)$ coordinates is $\omega \equiv dp/dt$, the time rate of change of pressure experienced by air parcels as they move along their three-dimensional trajectories through the atmosphere. Because pressure increases in the downward direction, positive $\omega$ denotes sinking motion and vice versa. Typical amplitudes of vertical velocity perturbations in the middle troposphere, for example, in baroclinic waves, are $\sim$100 hPa day$^{-1}$. At this rate it would take about a week for an air parcel to rise or sink through the depth of the troposphere.

The $(x, y, p)$ and $(x, y, z)$ vertical velocities $\omega$ and $w$ are related by the chain rule (1.3)

$$\omega \equiv \frac{dp}{dt} = \frac{\partial p}{\partial t} + \mathbf{V} \cdot \nabla p + w\frac{\partial p}{\partial z}$$

Substituting for $dp/dz$ from the hydrostatic equation (3.17) yields

$$\omega = -\rho g w + \frac{\partial p}{\partial t} + \mathbf{V} \cdot \nabla p \tag{7.32}$$

This relation can be simplified to derive an approximate linear relationship between $\omega$ and $w$. Typical local time rates of change of pressure in extratropical weather systems are $\sim$10 hPa day$^{-1}$ or less and the term $\mathbf{V} \cdot \nabla p$ tends to be even smaller due to the quasi-geostrophic character of large-scale atmospheric motions. Hence, to within $\sim$10%,

$$\omega \simeq -\rho g w \tag{7.33}$$

Based on this relationship, 100 hPa day$^{-1}$ is roughly equivalent to 1 km day$^{-1}$ or 1 cm s$^{-1}$ in the lower troposphere and twice that value in the midtroposphere.

Within the lowest 1–2 km of the atmosphere, where $w$ and $\omega$ are constrained to be small due to the presence of the lower boundary, the smaller terms in (7.32) cannot be neglected. At the Earth's surface the geometric vertical velocity

$$w_s = \mathbf{V} \cdot \nabla z_s \tag{7.34}$$

where $z_s$ is the height of the terrain.

### 7.3.2 Hydrostatic Balance

In $(x, y, z)$ coordinates, Newton's second law for the vertical motion component is

$$\frac{dw}{dt} = -\frac{1}{\rho}\frac{\partial p}{\partial z} - g + C_z + F_z \tag{7.35}$$

where $C_z$ and $F_z$ are the vertical components of the Coriolis and frictional forces, respectively. For large-scale motions, in which virtually all the kinetic energy resides in the horizontal wind component, the vertical acceleration is so small in comparison to the leading terms in (7.35) that it is not practically feasible to calculate it. To within $\sim$1%, the upward directed pressure gradient force balances the downward pull of gravity, not only for mean atmospheric conditions, but also for the perturbations in $p$ and $\rho$ observed in association with large-scale atmospheric motions.[21] Hence, vertical equation of motion (7.35) can be replaced by the hydrostatic equation (3.17) or, in pressure coordinates, by the hypsometric equation (3.29).

### 7.3.3 The Thermodynamic Energy Equation

The evolution of weather systems is governed not only by dynamical processes, as embodied in Newton's second law, but also by thermodynamic processes as represented in the first law of thermodynamics. In its simplest form the first law is a prognostic equation relating to the time rate of change of temperature of an air parcel as it moves through the atmosphere. These changes in temperature affect the thickness pattern, which, together with appropriate boundary conditions, determines the distribution of

[21] For a rigorous scale analysis of the primitive equations, see J. R. Holton, *An Introduction to Dynamic Meteorology*, Fourth edition, Academic Press, p. 41–42 (2004).

geopotential $\Phi$ on pressure surfaces. Thus if the horizontal temperature gradient changes in response to diabatic heating, the distribution of the horizontal pressure gradient force $(-\nabla\Phi)$ in the horizontal equation of motion (7.9) will change as well.

The first law of thermodynamics in the form (3.46) can be written in the form

$$J\,dt = c_p dT - \alpha\,dp$$

where $J$ represents the diabatic heating rate in J kg s$^{-1}$ and $dt$ is an infinitesimal time interval. Dividing through by $dt$ and rearranging the order of the terms yields

$$c_p \frac{dT}{dt} = \alpha \frac{dp}{dt} + J$$

Substituting for $\alpha$ from the equation of state (3.3) and $\omega$ for $dp/dt$ and dividing through by $c_p$, we obtain the *thermodynamic energy equation*

$$\frac{dT}{dt} = \frac{\kappa T}{p}\omega + \frac{J}{c_p} \tag{7.36}$$

where $\kappa = R/c_p = 0.286$.

The first term on the right-hand side of (7.36) represents the rate of change of temperature due to adiabatic expansion or compression. A typical value of this term in °C per day is given by $\kappa T \delta p/p_m$, where $\delta p = \omega \delta t$ is a typical pressure change over the course of a day following an air parcel and $p_m$ is the mean pressure level along the trajectory. In a typical middle-latitude disturbance, air parcels in the middle troposphere ($p_m \sim$500 hPa) undergo vertical displacements on the order of 100 hPa day$^{-1}$. Assuming $T \sim 250$ K, the resulting adiabatic temperature change is on the order of 15 °C per day.

The second term on the right-hand side of (7.36) represents the effects of diabatic heat sources and sinks: absorption of solar radiation, absorption and emission of longwave radiation, latent heat release, and, in the upper atmosphere, heat absorbed or liberated in chemical and photochemical reactions. In addition, it is customary to include, as a part of the diabatic heating, the heat added to or removed from the parcel through the exchange of mass between the parcel and its environment due to unresolved scales of motion such as convective plumes. Throughout most of the troposphere there tends to be a considerable amount of cancellation between the various radiative terms so that the net radiative heating rates are less than 1 °C per day. Latent heat release tends to be concentrated in small regions in which it may be locally comparable in magnitude to the adiabatic temperature changes discussed earlier. The convective heating within the mixed layer can also be locally quite intense, e.g., where cold air blows over much warmer ocean water. However, throughout most of the troposphere, the sum of the diabatic heating terms in (7.36) is much smaller than the adiabatic temperature change term.

Using the chain rule (1.4), (7.36) may be expanded to obtain the Eulerian (or "local") time rate of change of temperature

$$\frac{\partial T}{\partial t} = -\mathbf{V}\cdot\nabla T + \left(\frac{\kappa T}{p} - \frac{\partial T}{\partial p}\right)\omega + \frac{J}{c_p} \tag{7.37}$$

The first term on the right-hand side of (7.37) may be recognized as the horizontal advection term defined in (7.5), and the second term is the combined effect of adiabatic compression and vertical advection. In Exercise 7.36 the reader is invited to show that when the observed lapse rate is equal to the dry adiabatic lapse rate, the term in parentheses in (7.37) vanishes. In a stably stratified atmosphere, $\partial T/\partial p$ must be less than in the adiabatic lapse rate, and thus the term in parentheses must be positive. It follows that sinking motion (or subsidence) always favors local warming and vice versa: the more stable the lapse rate, the larger the local rate of temperature increase that results from a given rate of subsidence.

If the motion is adiabatic ($J = 0$) and the atmosphere stably stratified, air parcels will conserve potential temperature as they move along their three-dimensional trajectories, carrying the potential temperature surfaces (or isentropes) with them. For steady state (7.37) reduces to

$$\frac{\omega}{V} = \frac{\partial T/\partial s}{(\kappa T/p - \partial T/\partial p)}$$

which requires that the slopes of the three-dimensional trajectories be identical to the slopes of the local isentropes.

Throughout most of the extratropical troposphere the trajectories typically slope about half as steeply as the isentropes. Hence the horizontal advection term tends to dominate and the motion has the effect of

flattening out the isentropes. In time, the isentropic surfaces would become completely flat, were it not for the meridional heating gradient, which is continually tending to lift them at high latitudes and depress them at low latitudes. The role of the horizontal advection term in producing rapid local temperature changes observed in association with extratropical cyclones is illustrated in the following exercise.

***Exercise 7.4*** During the time that a frontal zone passes over a station the temperature falls at a rate of 2 °C per hour. The wind is blowing from the north at 40 km $h^{-1}$ and temperature is decreasing with latitude at a rate of 10 °C per 100 km. Estimate the terms in (7.37), neglecting diabatic heating.

***Solution*** $\partial T/\partial t = 2\ ^\circ\text{C h}^{-1}$ and

$$-\mathbf{V}\cdot\nabla T = -v\frac{\partial T}{\partial y} = 40\ \text{km h}^{-1} \times \frac{10^\circ\text{C}}{100\ \text{km}}$$
$$= 4^\circ\text{C h}^{-1}$$

The temperature at the station is dropping only half as fast as the rate of horizontal temperature advection so large-scale subsidence must be warming the air at a rate of 2 °C $h^{-1}$ as it moves southward. It follows that the meridional slopes of the air trajectories must be half as large as the meridional slopes of the isentropes.

Within the tropical troposphere the relative magnitude of the terms in (7.37) is altogether different from that in the extratropics. Horizontal temperature gradients are much weaker than in the extratropics, so the horizontal advection term is unimportant and temperatures at fixed points vary little from one day to the next. In contrast, diabatic heating rates in regions of tropical convection are larger than those typically observed in the extratropics. Ascent tends to be concentrated in small rain belts such as the ITCZ, where warming due to the release of latent heat of condensation is almost exactly compensated by the cooling induced by the vertical velocity term in (7.37). The prevailing lapse rate throughout the tropical troposphere all the way from the top of the boundary layer up to around the 200-hPa level is nearly moist adiabatic so that the lifting of saturated air does not result in large temperature changes, even when the rate of ascent is very large. Within the much larger regions of slow subsidence, warming due to adiabatic compression is balanced by weak radiative cooling. ■

### 7.3.4 Inference of the Vertical Motion Field

The vertical motion field cannot be predicted on the basis of Newton's second law, but it can be inferred from the horizontal wind field on the basis of the *continuity equation*, which is an expression of the conservation of mass.

Air parcels expand and contract in response to pressure changes. In general, these changes in volume are of two types: those associated with sound waves, in which the momentum of the air plays an essential role, and those that occur in association with hydrostatic pressure changes. When the equation for the continuity of mass is formulated in $(x, y, p)$ coordinates, only the meteorologically relevant hydrostatic volume changes are taken into account.

Consider an air parcel shaped like a block with dimensions $\delta x$, $\delta y$, and $\delta p$, as indicated in Fig. 7.17. If the atmosphere is in hydrostatic balance, the mass of the block is given by

$$\delta M = \rho\,\delta x\,\delta y\,\delta z = \frac{-\delta x\,\delta y\,\delta p}{g}$$

Because the mass of the block is not changing with time,

$$\frac{d}{dt}(\delta x\,\delta y\,\delta p) = 0 \qquad (7.38)$$

or, in expanded form,

$$\delta y\,\delta p\frac{d}{dt}\delta x + \delta x\,\delta p\frac{d}{dt}\delta y + \delta x\,\delta y\frac{d}{dt}\delta p = 0.$$

Expanding the time rates of change of $\delta x$, $\delta y$, and $\delta p$ in terms of partial derivatives of the velocity components, as in the derivation of (7.2), it is readily shown that

$$\frac{\delta u}{\delta x} + \frac{\delta v}{\delta y} + \frac{\delta \omega}{\delta p} = 0 \qquad (7.39a)$$

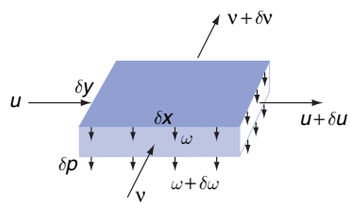


**Fig. 7.17** Relationships used in the derivation of the continuity equation.

or, in vectorial form,

$$\frac{\partial \omega}{\partial p} = -\nabla \cdot \mathbf{V} \tag{7.39b}$$

where $\nabla \cdot \mathbf{V}$ is the divergence of the horizontal wind field. Hence, horizontal divergence ($\nabla \cdot \mathbf{V} > 0$) is accompanied by vertical squashing ($\partial\omega/\partial p < 0$), and horizontal convergence is accompanied by vertical stretching, as illustrated schematically in Fig. 7.18.

Within the atmospheric boundary layer air parcels tend to flow across the isobars toward lower pressure in response to the frictional drag force. Hence, the low-level flow tends to converge into regions of low pressure and diverge out of regions of high pressure, as illustrated in Fig. 7.19. The frictional convergence within low-pressure areas induces ascent, while the divergence within high-pressure areas induces subsidence. In the oceans, where the Ekman drift is in the opposite sense, cyclonic, wind-driven gyres are characterized by *upwelling*, and anticyclonic gyres by *downwelling*. In a similar manner, regions of Ekman drift in the offshore direction are characterized by *coastal upwelling*, and the easterly surface winds along the equator induce a shallow Ekman drift away from the equator, accompanied by *equatorial upwelling*.


**Fig. 7.18** Algebraic signs of $\omega$ in the midtroposphere associated with convergence and divergence in the lower troposphere.

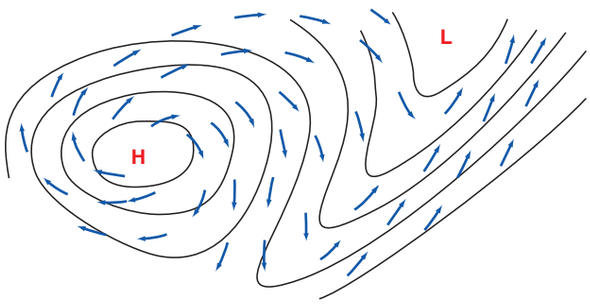


**Fig. 7.19** Cross-isobar flow at the Earth's surface induced by frictional drag. Solid lines represent isobars.

The vertical velocity at any given point $(x, y)$ can be inferred diagnostically by integrating the continuity equation (7.39b) from some reference level $p^*$ to level $p$,

$$\omega(p) = \omega(p^*) - \int_{p^*}^{p} (\nabla \cdot \mathbf{V})\, dp \tag{7.40}$$

In this form, the continuity equation can be used to deduce the vertical velocity field from a knowledge of the horizontal wind field. A convenient reference level is the top of the atmosphere, where $p^* = 0$ and $\omega = 0$. Integrating (7.40) downward from the top down to the Earth's surface, where $p = p_s$ we obtain

$$\omega_s = -\int_0^{p_s} (\nabla \cdot \mathbf{V})\, dp$$

Incorporating this result and (7.34) into (7.32) and rearranging, we obtain Margules'[22] *pressure tendency equation*

$$\frac{\partial p_s}{\partial t} = -\mathbf{V}_s \cdot \nabla p - w_s \frac{\partial p}{\partial z} - \int_0^{p_s} (\nabla \cdot \mathbf{V})\, dp \tag{7.41}$$

which serves as the bottom boundary condition for the pressure field in the primitive equations.

At the Earth's surface, the pressure tendency term $\partial p_s/\partial t$ is on the order of 10 hPa per day and the advection terms $-\mathbf{V}_s \cdot \nabla p_s$ and $-w_s(\partial p/\partial z)$ are usually even smaller. It follows that

$$\int_0^{p_s} (\nabla \cdot \mathbf{V})\, dp = p_s \{\nabla \cdot \mathbf{V}\} \sim 10 \text{ hPa day}^{-1}$$

where $\{\nabla \cdot \mathbf{V}\}$ is the mass-weighted, vertically-averaged divergence. Because $p_s \simeq 1000$ hPa and 1 day $\sim 10^5$ s, it follows that

$$\{\nabla \cdot \mathbf{V}\} \sim 10^{-7}\ \text{s}^{-1}$$

[22] **Max Margules** (1856–1920) Meteorologist, physicist, and chemist, born in the Ukraine. Worked in intellectual isolation on atmospheric dynamics from 1882 to 1906, during which time he made many fundamental contributions to the subject. Thereafter, he returned to his first love, chemistry. Died of starvation while trying to survive on a government pension equivalent to $2 a month in the austere post-World War I period. Many of the current ideas concerning the kinetic energy cycle in the atmosphere (see Section 7.4) stem from Margules' work.

That the vertically averaged divergence is typically about an order of magnitude smaller than typical magnitudes of the divergence observed at specific levels in the atmosphere reflects the tendency (first pointed out by Dines[23]) for compensation between lower tropospheric convergence and upper tropospheric divergence and vice versa. Vertical velocity $\omega$, which is the vertical integral of the divergence, tends to be strongest in the mid-troposphere, where the divergence changes sign.[24]

It is instructive to consider the vertical profile of atmospheric divergence in light of the idealized flow patterns for the two-dimensional flow in two different kinds of waves in a stably stratified liquid in which density decreases with height. Fig. 7.20a shows an idealized *external wave* in which divergence is independent of height and vertical velocity increases linearly with height from zero at the bottom to a maximum at the free surface of the liquid. Fig. 7.20b shows an *internal wave* in a liquid that is bounded by a rigid upper lid so that $w = 0$ at both top and bottom, requiring perfect compensation between low level convergence and upper level divergence and *vice versa*. In the Earth's atmosphere, motions that resemble the internal wave contain several orders of magnitude more kinetic energy than those that resemble the external wave. In some respects, the stratosphere plays the role of a "lid" over the troposphere, as evidenced by the fact that the geometric vertical velocity $w$ is typically roughly an order of magnitude smaller in the lower stratosphere than in the midtroposphere.

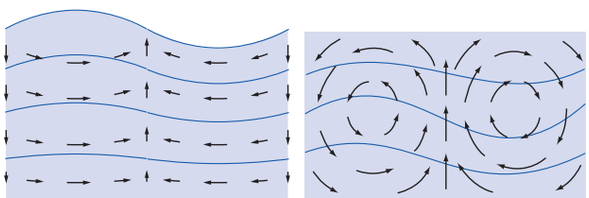


**Fig. 7.20** Motion field in a vertical cross section through a two-dimensional wave propagating from left to right in a stably stratified liquid. The contours represent surfaces of constant density. (a) An *external wave* in which the maximum vertical motions occur at the free surface of the liquid, and (b) an *internal wave* in which the vertical velocity vanishes at the top because of the presence of a rigid lid.

### 7.3.5 Solution of the Primitive Equations

The primitive equations, in the simplified form that we have derived them, consist of the horizontal equation of motion

$$\frac{d\mathbf{V}}{dt} = -\nabla\Phi - f\mathbf{k} \times \mathbf{V} + \mathbf{F} \tag{7.14}$$

the hypsometric equation

$$\frac{\partial\Phi}{\partial p} = \frac{-RT}{p} \tag{3.23}$$

the thermodynamic energy equation

$$\frac{dT}{dt} = \frac{\kappa T}{p}\omega + \frac{J}{c_p} \tag{7.36}$$

and the continuity equation

$$\frac{\partial\omega}{\partial p} = -\nabla \cdot \mathbf{V} \tag{7.39b}$$

together with the bottom boundary condition

$$\frac{\partial p_s}{\partial t} = -\mathbf{V}_s \cdot \nabla p - w_s\frac{\partial p}{\partial z} - \int_0^{p_s} (\nabla \cdot \mathbf{V})\, dp \tag{7.41}$$

Bearing in mind that the horizontal equation of motion is made up of two components, the system of primitive equations, as presented here, consist of five equations in five dependent variables: $u$, $v$, $\omega$, $\Phi$, and $T$. The fields of diabatic heating $J$ and friction $\mathbf{F}$ need to be prescribed or *parameterized* (i.e., expressed as functions of the dependent variables). The horizontal equation(s) of motion, the thermodynamic energy equation, and the equation for pressure on the bottom boundary all contain time derivatives and are

[23] **Willam Henry Dines** (1855–1927) British meteorologist. First to invent a device for measuring both the direction and the speed of the wind (the Dines' pressure-tube anemometer). Early user of kites and ballons to study upper atmosphere.

[24] The midtroposphere minimum in the amplitude of $\nabla \cdot \mathbf{V}$ justifies the use of (7.22) in diagnosing the vorticity balance at that level. Alternatively, (7.22) can be viewed as relating to the vertically averaged tropospheric wind field, whose vorticity is two orders smaller than its divergence.

therefore said to be *prognostic equations*. The remaining so-called *diagnostic equations* describe relationships between the dependent variables that apply at any instant in time.

The primitive equations can be solved numerically. The dependent variables are represented on an array of regularly spaced horizontal grid points and at a number of vertical levels. In global models, the grid points usually lie along latitude circles and meridians, although the latitudinal spacing is not necessarily uniform. The equations are converted to the Eulerian form (1.4) so that the calculations can be performed on a fixed set of grid points and levels rather than requiring the grid to move with the air trajectories. Initial conditions for the dependent variables are specified at time $t_0$, taking care to ensure that the diagnostic relations between the variables are satisfied (e.g., the geopotential field must be hydrostatically consistent with the temperature field).

Terms in the equations involving horizontal and vertical derivatives are evaluated using *finite difference techniques* (approximating them as differences between the numerical values of the respective variables at neighboring grid points and levels in the array divided by the distances between the grid points) or as the coefficients of a mutually orthogonal set of analytic functions called *spherical harmonics*.[25] The time derivative terms $\partial V/\partial t$, $\partial T/\partial t$, and $\partial p_s/\partial t$ are then evaluated and their respective three-dimensional fields are projected forward through a short time step $\Delta t$ so that, for example,

$$u(t_0 + \Delta t) = u(t_0) + \frac{\partial u}{\partial t}\Delta t$$

The diagnostic equations are then applied to obtain dynamically consistent fields of the other dependent variables at time $t_0 + \Delta t$. The process is then repeated over a succession of time steps to describe the evolution of the fields of the dependent variables.

The time step $\Delta t$ must be short enough to ensure that the fields of the dependent variables are not corrupted by spurious small scale patterns arising from numerical instabilities. The higher the spatial resolution of the model, the shorter the maximum allowable time step and the larger the number of calculations required for each individual time step. Hence the computer resources required for numerical weather prediction and climate modeling increase sharply with the spatial resolution of the models.

### 7.3.6 An Application of Primitive Equations

To show how the dynamic processes represented in the primitive equations give rise to atmospheric motions and maintain them in the presence of friction, let us consider the events that transpire during the first few time steps when an atmospheric primitive equation model is "turned on," starting from a state of rest. Initially the atmosphere is stably stratified and the pressure and potential temperature surfaces are horizontally uniform.

Starting at time $t = 0$, the tropics begin to warm and the polar regions begin to cool in response to an imposed distribution of diabatic heating, which is designed to mimic the equator-to-pole heating gradient in the real atmosphere. As the tropical atmosphere warms, thermal expansion causes the pressure surfaces in the upper troposphere to bulge upward, while cooling of the polar atmosphere causes the pressure surfaces to bend downward as depicted in Fig. 7.21a. These tendencies are evident even in the very first time step of the time integration. The sloping of the pressure surfaces gives rise to an equator-to-pole pressure gradient at the upper levels. The pressure gradient force, in turn, drives the poleward flow depicted in Fig. 7.21a, which comes into play in the second time step of the integration.

The poleward mass flux results in a latitudinal redistribution of mass, causing surface pressure to drop in low latitudes and rise in high latitudes. The resulting low level equator-to-pole pressure gradient drives a compensating equatorward low level flow. Hence, the initial response to the heating gradient is the development of an equator-to-pole circulation cell, as shown in Fig. 7.21b. The Coriolis force in the horizontal equation of motion imparts a westward component to the equatorward flow in the lower branch of the cell and an eastward component to the poleward flow in the upper branch, as shown in Fig. 7.21c.

[25] *Spherical harmonics* are products of Legendre polynomials in the latitude domain and sines and cosines in the longtitude domain. In the spherical harmonic representation of the primitive equations, operations such as taking horizontal gradients ($\partial/\partial x$, $\partial/\partial y$), Laplacians ($\nabla^2$), and inverse Laplacians ($\nabla^{-2}$) reduce to simple algebraic operations performed on the coefficients.

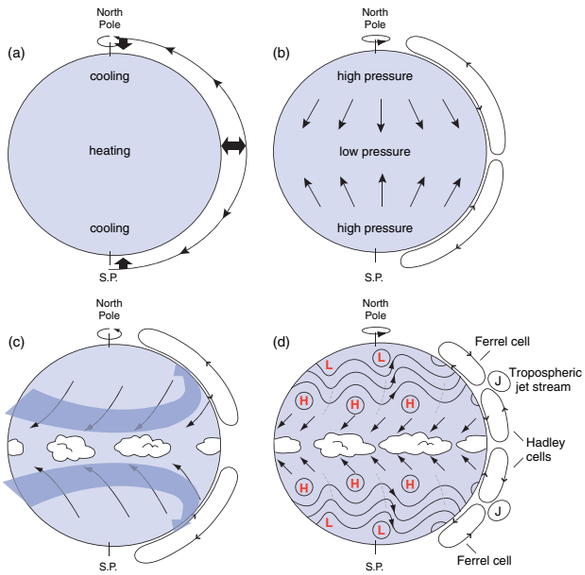


**Fig. 7.21** Schematic depiction of the general circulation as it develops from a state of rest in a climate model for equinox conditions in the absence of land–sea contrasts. See text for further explanation.

The flow becomes progressively more zonal with each successive time step, until the meridional component of the Coriolis force comes into geostrophic balance with the pressure gradient force, as illustrated in Fig. 7.22. As required by thermal wind balance, the vertical wind shear between the low level easterlies and the upper level westerlies increases in proportion to the strengthening equator-to-pole temperature gradient forced by the meridional gradient of the diabatic heating. The Coriolis force acting on the relatively weak meridional cross-isobar flow is instrumental in building up the vertical shear. Frictional drag limits the strength of the surface easterlies, but the westerlies aloft become stronger with each successive time step. Will these runaway westerlies continue to increase until they become supersonic

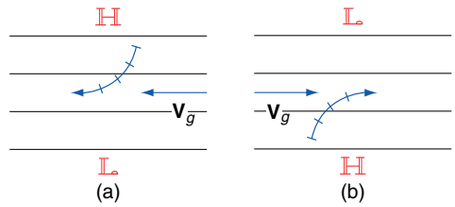


**Fig. 7.22** Trajectories of air parcels in the middle latitudes of the northern hemisphere near the Earth's surface (left) and in the upper troposphere (right) during the first few time steps of the primitive equation model integration described in Fig. 7.21. The solid lines represent geopotential height contours and the curved arrows represent air trajectories.

or will some as yet to be revealed process intervene to bring them under control? The answer is reserved for the following section.

## 7.4 The Atmospheric General Circulation

Dating back to the pioneering studies of Halley[26] in 1676 and Hadley in 1735, scientists have sought to explain why the surface winds blow from the east at subtropical latitudes and from the west in middle latitudes, and why the trade winds are so steady from one day to the next compared to the westerlies in midlatitudes. Such questions are fundamental to an understanding of the atmospheric *general circulation*; i.e., the statistical properties of large-scale atmospheric motions, as viewed in a global context.

Two important scientific breakthroughs that occurred around the middle of the 20th century paved the way for a fundamental understanding of the general circulation. The first was the simultaneous discovery of *baroclinic instability* (the mechanism that gives rise to baroclinic waves and their attendant extratropical cyclones) by Eady[27] and Charney.[28] The second was the advent of *general circulation models*: numerical

[26] **Edmund Halley** (1656–1742) English astronomer and meteorologist. Best known for the comet named after him. Determined that the force required to keep the planets in their orbits varies as the inverse square of their respective distances from the sun. (It remained for Newton to prove that the inverse square law yields elliptical paths, as observed.) Halley undertook the business and printing ("at his own charge") of Newton's masterpiece *the Principia*. First to derive a formula relating air pressure to altitude.

[27] **E. T. Eady** (1915–1966) English mathematician and meteorologist. Worked virtually alone in developing a theory of baroclinic instability while an officer on the Royal Air Force during World War II. One of us (P. V. H.) is grateful to have had him as a tutor.

[28] **Jule G. Charney** (1917–1981) Made major contributions to the theory of baroclinic waves, planetary-waves, tropical cyclones, and a number of other atmospheric and oceanic phenomena. While working at the Institute for Advanced Studies at Princeton University he helped lay the groundwork for numerical weather prediction. Later served as professor at Massachusetts Institute of Technology where one of us (J. M. W.) is privileged to have had the opportunity to learn from him. Played a prominent role in fostering large international programs designed to advance the science of weather prediction.

models of the global atmospheric circulation based on the primitive equations that can be run over long enough time intervals to determine seasonally varying, climatological mean winds and precipitation, the degree of steadiness of the winds, etc.

The importance of these developments becomes apparent if we extend the numerical integration described in the last section forward in time, based on results that have been replicated in many different general circulation models (GCM's). The ensuing developments could never have been anticipated on the basis of the simple dynamical arguments presented in the previous section. When the meridional temperature gradient reaches a critical value, the simulated circulation undergoes a fundamental change: baroclinic instability spontaneously breaks out in midlatitudes, imparting a wave-like character to the flow. The baroclinic waves create and maintain the circulation in the configuration indicated in Fig. 7.21d. In the developing waves, warm, humid subtropical air masses flow poleward ahead of the eastward moving surface cyclones, while cold, dry polar air masses flow equatorward behind the cyclones. The exchange of warm and cold air masses across the 45° latitude circle results in a net poleward flux of sensible and latent heat, arresting the buildup of the equator-to-pole temperature gradient.

Successive generations of baroclinic waves develop and evolve through their life cycles, emanating from their source region in the midlatitude lower troposphere, first dispersing upward toward the jet stream (~10 km) level and thence equatorward into the tropics. The equatorward dispersion of the waves in the upper troposphere causes the axes of their ridges and troughs to tilt in the manner shown in Fig. 7.21d. As a consequence of this tilt, poleward-moving air to the east of the troughs exhibits a stronger westerly wind component than equatorward moving air to the west of the troughs. The difference in the amount of westerly momentum carried by poleward and equatorward moving air parcels gives rise to a net poleward flux of westerly momentum from the subtropics into middle latitudes. In response to the import of westerly momentum from the subtropics, the surface winds in midlatitudes shift from easterly (Fig. 7.21c) to westerly (Fig. 7.21d), the direction of the midlatitude surface winds in the real atmosphere.

Baroclinic waves drive their own weak northern and southern hemisphere mean meridional circulation cells, referred to as *Ferrel*[29] *cells*, characterized by poleward, frictionally induced Ekman drift at the latitude of the storm tracks (~45°), ascent on the poleward flank, and descent on the equatorward flank, as indicated in Fig. 7.21d. Hence, with the spontaneous development of the baroclinic waves, the Hadley cells withdraw into the tropics, and a region of subsidence develops at subtropical (~30°) latitudes. These regions of subsidence coincide with the subtropical anticyclones (Figs. 1.18 and 1.19), which mark the boundary between the tropical trade winds and the extratropical westerlies. Most of the world's major desert regions lie within this latitude belt.

### 7.4.1 The Kinetic Energy Cycle

Frictional dissipation observed within the planetary boundary layer and within patches of turbulence within the free atmosphere continually depletes the kinetic energy of large-scale wind systems. Half the energy would be gone within a matter of days were there not some mechanism operating continually to restore it. The ultimate source of this kinetic energy is the release of potential energy through the sinking of colder, denser air and the rising of warmer, less dense air, which has the effect of lowering the atmosphere's center of mass, flattening the potential temperature surfaces, and weakening the existing horizontal temperature gradients. A simple steady-state laboratory analog of the kinetic energy cycle is depicted schematically in Fig. 7.23.

In small-scale convection, the kinetic energy generated by the rising of buoyant plumes is imparted to the vertical component of the motion. The upward buoyancy force disturbs the balance of forces in the vertical equation of motion, inducing vertical accelerations. The vertical overturning that occurs in association with large-scale atmospheric motions cannot be viewed as resulting from buoyancy forces because, in the primitive equations, the vertical equation of motion is replaced by the hydrostatic equation, which has no vertical acceleration term. In large-scale motions, kinetic energy is imparted directly to the horizontal wind field. When warm air rises and

[29] **William Ferrel** (1817–1891) American scientist. A schoolteacher early in his career and later held positions at the Nautical Almanac Office, the Coast Survey, and the Signal Office, which housed the Weather Bureau. Was the first to correctly deduce that gravitational tides retard the earth's rotation, and to explain the profound influence of the Coriolis force on winds and ocean currents that leads to geostrophic flow, as articulated in Buys Ballot's law.

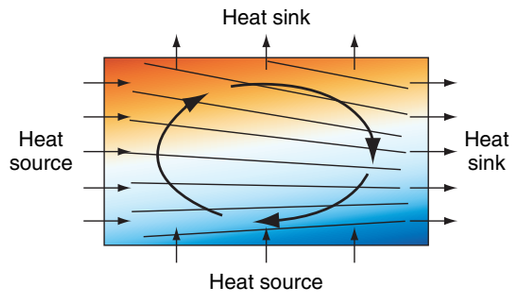


**Fig. 7.23** Vertical cross section through a steady-state circulation in the laboratory, driven by the distribution of heat sources and heat sinks as indicated. The colored shading indicates the distribution of temperature and density, with cooler, denser fluid represented by blue. The sloping black lines represent pressure surfaces. Note that the flow is directed down the horizontal pressure gradient at both upper and lower levels.

cold air sinks, the potential energy that is released does work on the horizontal wind field by forcing it to flow across the isobars from higher toward lower pressure. In the equation for the time rate of change of kinetic energy,

$$\mathbf{V} \cdot \frac{d\mathbf{V}}{dt} = \frac{d}{dt}\frac{V^2}{2} = -\mathbf{V} \cdot \nabla\Phi + \mathbf{F} \cdot \mathbf{V} \qquad (7.42)$$

the cross-isobar flow $-\mathbf{V} \cdot \nabla\Phi$ is the one and only source term. Flow across the isobars toward lower pressure is prevalent close to the Earth's surface, where the dissipation term $\mathbf{F} \cdot \mathbf{V}$ is most intense. Frictional drag is continually acting to reduce the wind speed, causing it to be subgeostrophic, so that the Coriolis force is never quite strong enough to balance the pressure gradient force. The imbalance drives a cross-isobar flow toward lower pressure (Fig. 7.19), which maintains the kinetic energy and the surface wind speed in the presence of frictional dissipation. This process is represented by the second term on the right-hand side of (7.42). It can be shown that, in the integral over the entire mass of the atmosphere, the generation of kinetic energy by the $-\mathbf{V} \cdot \nabla\Phi$ term in (7.42) is equal to the release of potential energy associated with the rising of warm air and sinking of cold air.[30]

The trade winds in the lower branch of the Hadley cell are directed down the pressure gradient, out of the subtropical high pressure belt and into the belt of low pressure at equatorial latitudes. That the winds in the upper troposphere blow from west to east implies that $\Phi$ decreases with latitude at that level, and hence that the poleward flow in the upper branch of the Hadley cell is also directed down the pressure gradient.

Closed circulations like the Hadley cell, which are characterized by the rising of warmer, lighter air and the sinking of colder, denser air and the prevalence of cross-isobar horizontal flow toward lower pressure, release potential energy and convert it to the kinetic energy of the horizontal flow. Circulations with these characteristics are referred to as *thermally direct* because they operate in the same sense as the global kinetic energy cycle. Other examples of thermally direct circulations in the Earth's atmosphere are the large-scale overturning cells in baroclinic waves, monsoons and tropical cyclones. Circulations such as the Ferrel cell, that operate in the opposite sense, with rising of colder air and sinking of warmer air are referred to as *thermally indirect*.

Because thermally direct circulations are continually depleting the atmosphere's reservoir of potential energy, something must be acting to restore it. Heating of the atmosphere by radiative transfer and the release of the latent heat of condensation of water vapor in clouds is continually replenishing the potential energy in two ways: by warming the atmosphere in the tropics and cooling it at higher latitudes and by heating the air at lower levels and cooling the air at higher levels. The former acts to maintain the equator-to-pole temperature contrast on pressure surfaces, and the latter expands the air in the lower troposphere and compresses the air in the upper troposphere, thereby lifting the air at intermediate levels, maintaining the height of the atmosphere's center of mass against the lowering produced by thermally direct circulations. Hence, the maintenance of large-scale atmospheric motions requires both horizontal and vertical heating gradients analogous to those in the laboratory experiment depicted in Fig. 7.23. In contrast, the maintenance of convection requires only vertical heating gradients.

The most important heat source in the troposphere is the release of latent heat of condensation that occurs in association with precipitation. Latent heat

[30] A formal proof of this relationship is beyond the scope of this text, but a simple analog that contains all the essential elements in the proof is presented in Exercise 7.46.

release tends to occur preferentially in rising air, which becomes saturated as it cools adiabatically. This preferential heating of the rising air tends to maintain and enhance the horizontal temperature gradients that drive thermally direct circulations, rendering the motions more vigorous than they would be in a dry atmosphere. Condensation heating plays a supporting role as an energy source for extratropical cyclones and it plays a starring role in the energetics of tropical cyclones.

The *kinetic energy cycle* can be summarized in terms of the flowchart presented in Fig. 7.24. Potential energy generated by heating gradients is converted to kinetic energy of both large-scale and smaller scale convective motions. Kinetic energy is drained from the large-scale reservoir by shear instability and flow over rough surfaces, both of which generate small-scale turbulence and wave motions, as discussed in Chapter 9. Kinetic energy in the small-scale reservoir is transferred to smaller and smaller scales until it becomes indistinguishable from random molecular motions and thus becomes incorporated into the atmosphere's reservoir of internal energy. This final step is represented in Fig. 7.24 as "a drop in the bucket" to emphasize that it is a small contribution to the atmosphere's vast internal energy reservoir: only locally in regions of very strong winds such as those near the centers of tropical cyclones is frictional dissipation strong enough to affect the temperature.

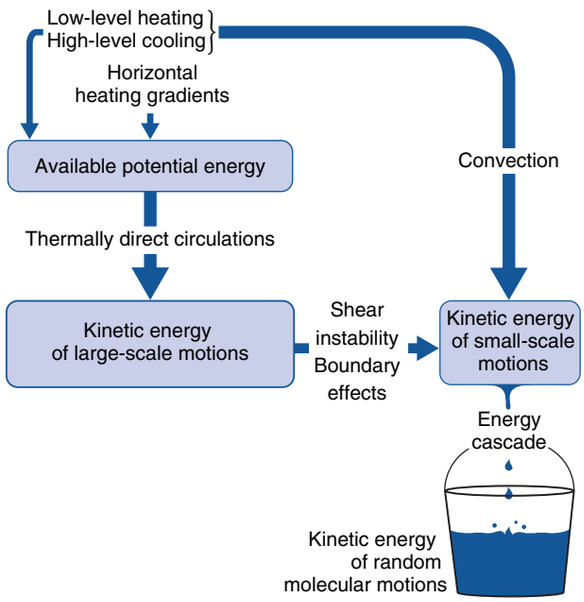


**Fig. 7.24** Schematic flow diagram for the kinetic energy cycle in the atmospheric general circulation.

### 7.4.2 The Atmosphere as a Heat Engine

The primary tropospheric heat sources tend to be concentrated within the planetary boundary layer, as discussed in the previous chapter, and in regions of heavy precipitation. The primary heat sink, radiative cooling in the infrared, is more diffuse. In a gross statistical sense, the center of mass of the heating is located at a slightly lower latitude and at a slightly lower altitude than the center of mass of the cooling, and is therefore at a somewhat higher temperature. The atmospheric general circulation can be viewed as a heat engine that is continually receiving heat at a rate $Q_H$ at that higher temperature $T_H$ and rejecting heat at a rate $Q_C$ at the lower temperature $T_C$. By analogy with (3.77) for the Carnot cycle, we can write an expression for the thermal efficiency of the atmospheric heat engine

$$\eta = \frac{W}{Q_H} \tag{7.43}$$ [AU1]

where $W$ is the rate at which work is done in generating kinetic energy in thermally direct circulations. The integral of the kinetic energy generation term $-\mathbf{V} \cdot \nabla\Phi$ over the mass of the atmosphere is estimated to be ~1–2 W m$^{-2}$. $Q_H$, the net incoming solar radiation averaged over the surface of the Earth, is ~240 W m$^{-2}$. Hence, based on this definition, the thermal efficiency of the atmospheric heat engine is less than 1%. In contrast to the situation in the Carnot cycle, much of the heat transfer that takes place within the atmosphere is irreversible. For example, cold, polar air masses that penetrate into the tropics are rapidly modified by the heat fluxes from the underlying surfaces and radiative transfer. It follows that relationships derived from the reversible Carnot cycle are not strictly applicable to the atmospheric heat engine.

## 7.5 Numerical Weather Prediction

Until the 1950s, day-to-day weather forecasting was largely based on subjective interpretation of synoptic charts. From the time of the earliest synoptic networks, it has been possible to make forecasts by extrapolating the past movement of the major features on the charts. As forecasters began to acquire experience from a backlog of past weather situations, they were able to refine their forecasts somewhat by making use of historical analogs of the current weather situation, without reference to the underlying dynamical principles introduced in this chapter. However, it soon became

apparent that the effectiveness of this so-called "analog technique" is inherently limited by the unavailability of very close analogs in the historical records. On a global basis the three-dimensional structure of the atmospheric motion field is so complicated that a virtually limitless number of distinctly different flow patterns are possible, and hence the probability of two very similar patterns being observed, say, during the same century, is extremely low. By 1950 the more advanced weather forecasting services were already approaching the limit of the skill that could be obtained strictly by the use of empirical techniques.

The earliest attempts at numerical weather prediction, based on the methodology described in Section 7.2.9, date back to the 1950s and primitive equation models came into widespread use soon afterward. In comparison to the models developed in these pioneering efforts, today's numerical weather prediction models have much higher spatial resolution and contain a much more accurate and detailed representation of the physical processes that enter into the primitive equations. The increase in the physical complexity of the models would not have been possible without the rapid advances in computer technology that have taken place during the past 50 years: to make a single forecast for 1 day in advance by running current operational models on a computer of the type available 50 years ago would require millennia of computer time! The payoff of this monumental effort is the remarkable improvement in forecast skill documented in Fig. 1.1.

The initial conditions for modern numerical weather prediction are based on an array of global observations, an increasing fraction of which are remote measurements from radiometers carried on board satellites. In situ observations include surface reports, radiosonde data, and flight level data from commercial aircraft. In situ measurements of pressure, wind, temperature, and moisture are combined with satellite-derived radiances in dynamically consistent, multivariate *four-dimensional data assimilation systems* like the one described in Box 8.1.

The global observing system describes only the resolvable scales of atmospheric variability, and the analysis is subject to measurement errors even at the largest scales. The data assimilation scheme is designed to correct for the systematic errors in the observations and to minimize the impact of random errors on the forecasts. The errors in the initial conditions for numerical weather prediction have been continually shrinking in response to a host of incremental improvements in the observing and data assimilation systems. Nevertheless, there will always remain some degree of uncertainty (or errors) in the initial conditions and, due to the nonlinearity of atmospheric motions, these errors inevitably amplify with time. Beyond some threshold forecast interval the forecast fields are, on average, no more like the observed fields against which they are verified than two randomly chosen observed fields for the same time of year are like one another.[31] For the extratropical atmosphere this so-called *limit of deterministic predictability* is believed to be on the order of 2 weeks.[32]

Figure 7.25 shows a set of forecasts, made on successive days, for the same time, together with the *verifying analysis* (i.e., the corresponding "observed"[33] fields for the time that matches the forecast). This particular example was chosen because the level of skill is typical of wintertime forecasts made with today's state-of-the art numerical weather prediction systems. Forecast skill declines monotonically as the forecast interval lengthens. The 1- and 3-day forecasts replicate the features in the verifying analysis with a high degree of fidelity; the 7-day forecast still captures all the major features in the field, but misses many of the finer details. The 10-day forecast is worthless over much of the hemisphere, but even at this long lead time, the more prominent features in the verifying analysis are already apparent over the Atlantic, European, and western North American sectors.

The increase in the uncertainty of the forecasts with increasing forecast interval is illustrated in Fig. 7.26 in the context of a simplified forecast model based on the *Lorenz attractor* described in Box 1.1. In the first experiment shown in the left panel, the initial conditions that make up the ensemble lie within a region of the attractor for which the forecast uncertainty actually declines for a while as the numerical integration

[31] Measures of similarity and dissimilarity between fields are explored in Exercise 7.47.

[32] The atmosphere is not the only system whose future evolution (beyond some threshold time) is exquisitely sensitive to initial conditions. A pool shot involving multiple collisions exhibits an analogous sensitivity: with each collision the uncertainty inherent in the initial position and speed of the cue ball is multiplied by a large factor. Beyond about seven collisions, the uncertainty inherent in the initial conditions that exists by virtue of the Heisenberg uncertainty principle precludes the possibility of predicting the outcome of the shot!

[33] The "observed" fields are derived from data assimilation schemes like the one described in Box 8.1.

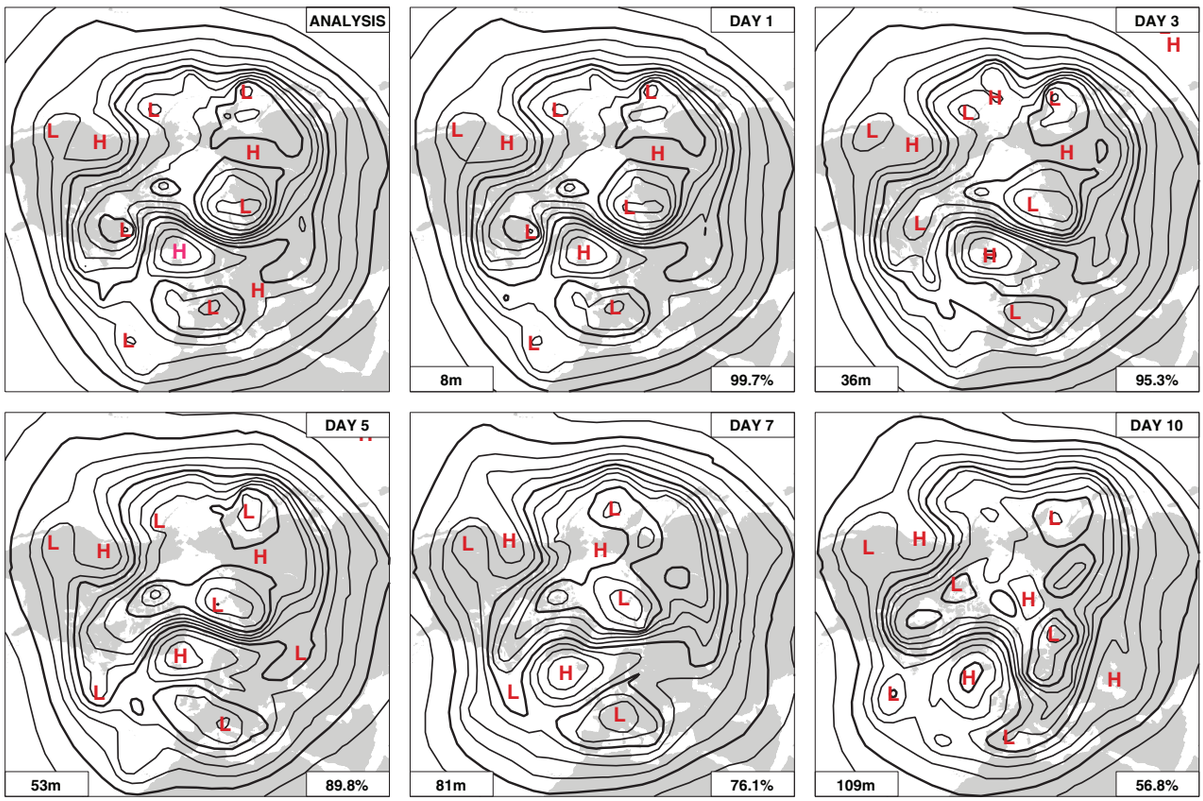


**Fig. 7.25** Forecasts and verifying analysis of the northern hemisphere 500-hPa height field for 00 UTC February 24, 2005. The number printed in the lower left corner is the *root mean squared* error and the percentage shown in the lower right corner of each panel is the *anomaly correlation*, a measure of the hemispherically averaged skill of the forecast. [Courtesy of Adrian J. Simmons, European Centre for Medium Range Weather Forecasts (ECMWF).]

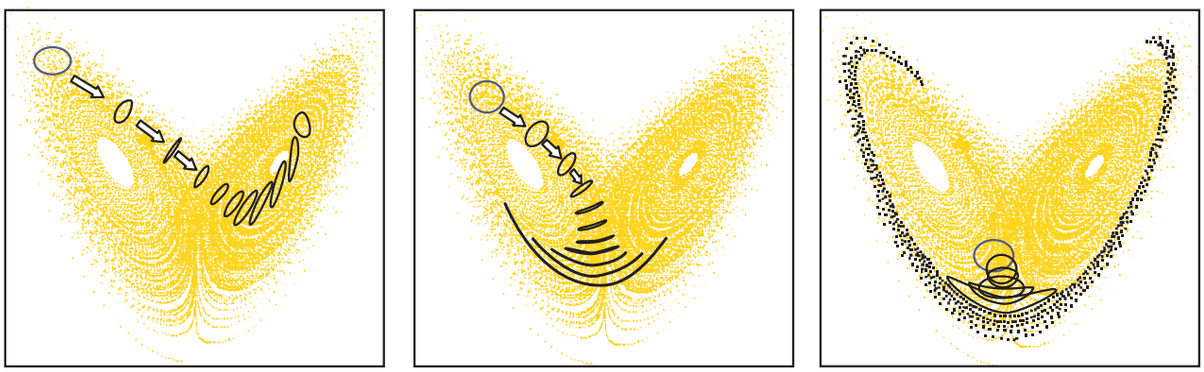

**Fig. 7.26** Three sets of *ensemble forecasts* performed using the highly simplified three-variable representation of the atmosphere described in Box 1.1. The time-dependent solution of the governing governing equations traces out the three-dimensional geometric pattern, referred to as the *Lorenz attractor*. Each panel represents a numerical experiment in which the initial conditions are the ensemble of points that lie along the purple ellipse at the upper right and the forecasts at successive forecast times are represented by the "down-stream" black ellipses. Each point on the ellipse of initial conditions is uniquely identified with a point on each of the successive forecast ellipses. The increasing size of the forecast ellipses with lengthening of the forecast interval in the center and right panels reflects the growth of uncertainty in the forecasts. In the third experiment, represented in the right panel, the spread of the members of the ensemble becomes so large that the forecast ellipse loses its identity. [Courtesy of T. N. Palmer, ECMWF.]

proceeds, as evidenced by the decreasing size of successive forecast ellipses. In the second experiment (middle panel), successive forecast ellipses widen markedly as the points representing the individual forecasts that make up the ensemble approach the bottom of the attractor and spread out into the two separate loops. In the third experiment (right panel) the rapid increase in the uncertainty of the forecasts begins earlier in the forecast interval, and the points along the bottom of the attractor spread rapidly around their respective loops as the forecast proceeds. Hence the predictability of this simple model is highly dependent on the initial state.

Ensemble forecasts carried out with the full set of governing equations for large-scale atmospheric motions provide a means of estimating the uncertainties inherent in weather forecasts at the time when they are issued. The results are not as easy to interpret as those for the idealized model based on the Lorenz attractor, but they are nonetheless informative. As in the idealized experiments, the ensemble forecasts also provide an indication of the range of atmospheric states that could develop out of the observed initial conditions. In current operational practice, different forecast models, as well as perturbed initial conditions, are used to generate different members of the ensemble. At times when the entire hemispheric circulation is relatively predictable, members of the ensemble do not diverge noticeably from one another until relatively far into the forecast. Often the errors grow most rapidly over one particular sector of the hemisphere due to the presence of local instability in the hemispheric flow pattern. The rate of divergence of the individual members of the ensemble provides a measure of the credibility of the forecasts in various sectors of the hemisphere and the length of the time interval over which the forecasts can be trusted.

Figure 7.27 shows 7-day ensemble forecasts for a typical winter day. The mean is considerably smoother than its counterpart in Fig. 7.25 because it represents an average over many individual forecasts. Some of the individual forecasts, like the one in the lower left panel, capture the features in the verifying analysis with remarkable fidelity. Unfortunately, there is no way of identifying these highly skillful forecasts at the time that the ensemble forecast is made.

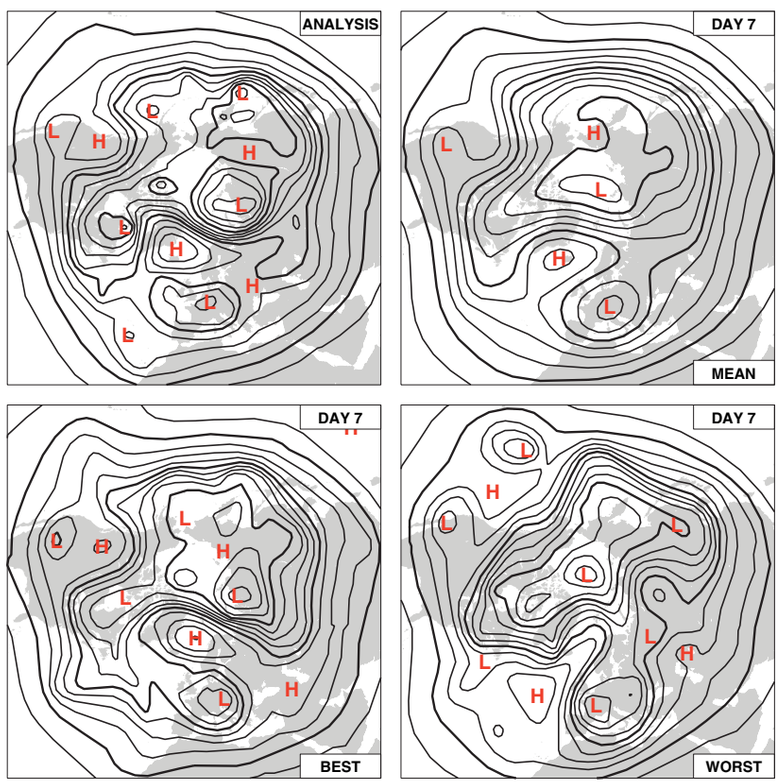


**Fig. 7.27** As in Fig. 7.25 but for the 7-day forecasts generated by the ensemble forecasting system in current use at ECMWF. *Mean* is the average of the 50 members of the ensemble *Best* and *Worst* forecasts are selected based on anomaly correlations with the verifying analysis. [Courtesy of Adrian J. Simmons, ECMWF.]

## Exercises

7.5 Explain or interpret the following on the basis of the principles discussed in this chapter.

(a) A diffluent flow does not necessarily exhibit divergence.

(b) A flow with horizontal shear does not necessarily exhibit vorticity.

(c) A person of fixed mass weighs slightly less when flying on an eastbound plane than when flying on a westbound plane.

(d) A satellite can be launched in such a way that it remains overhead at a specified longitude directly over the equator in a so called *geostationary orbit*.

(e) The oblateness of the shape of Jupiter is more apparent than that of the Earth.

(f) The Coriolis force has no discernible effect on the circulation of water going down the drain of a sink.

(g) The vertical component of the Coriolis force is not important in atmospheric dynamics, nor is the Coriolis force induced by vertical motions.

(h) The strong winds encircling hurricanes are highly subgeostrophic.

(i) Cyclones tend to be more intense than anticyclones.

(j) The wind in valleys usually blows up or down the valley from higher toward lower pressure rather than blowing parallel to the isobars.

(k) Surface winds are usually closer to geostrophic balance over oceans than over land.

(l) When high and low cloud layers are observed to be moving in different directions, it can be inferred that horizontal temperature advection is occurring.

(m) Veering of the wind with height within the planetary boundary layer is not necessarily an indication of warm advection.

(n) Areas of precipitation tend to be associated with convergence in the lower troposphere and divergence in the upper troposphere.

(o) The estimation of divergence from wind observations is subject to larger percentage errors than the estimation of vorticity.

(p) The pressure gradient force does not affect the circulation around any closed loop that lies on a pressure surface.

(q) Motions in the middle troposphere tend to be quasi-nondivergent.

(r) The primitive equations assume a simpler form in pressure coordinates than in height coordinates.

(s) The thermodynamic energy equation assumes a particularly simple form in isentropic coordinates.

(t) In middle latitudes, local rates of change of temperature tend to be smaller than the changes attributable to horizontal temperature advection.

(u) Temperatures do not always rise in regions of warm advection.

(v) The release of latent heat in the midtroposphere has the effect of increasing the isentropic potential vorticity of the air in the column below it.

(w) Rising of warm air and sinking of cold air result in the generation of kinetic energy, even in hydrostatic motions.

(x) The Hadley cell does not extend from equator to pole.

(y) A term involving the Coriolis force does not appear in Eq. (7.42).

(z) The easterlies in the lower branch of the Hadley cell are maintained in the presence of friction.

(aa) Baroclinic waves and monsoons tend to be more vigorous in general circulation models that incorporate the effects of moisture than in those that do not.

(bb) Hydroelectric power may be viewed as a by-product of the atmospheric general circulation.

7.6 Describe the vorticity distribution within a flow characterized by counterclockwise circular flow with tangential velocity $u$ inversely proportional to radius $r$.

***Solution:*** The radial velocity profile is $ur = k$, where $k$ is a constant. Hence the contribution of the shear to the vorticity is $d(k/r)/dr = -k/r^2$, and the contribution of the curvature is $(k/r)/r = +k/r^2$. As in Exercise 7.1, the contributions are of equal absolute magnitude, but in this case they cancel so $\zeta = 0$ everywhere except at the center of the circle where the flow is undefined and the vorticity is infinite.

Such a flow configuration is referred to as an *irrotational vortex*. ■

7.7 At a certain location along the ITCZ, the surface wind at 10 °N is blowing from the east–northeast (ENE) from a compass angle of 60° at a speed of 8 m $s^{-1}$ and the wind at 7 °N is blowing from the south–southeast (SSE) (150°) at a speed of 5 m $s^{-1}$. (a) Assuming that $\partial/\partial y \gg \partial/\partial x$, estimate the divergence and the vorticity averaged over the belt extending from 7 °N to 10 °N. (b) The meridional component of the wind drops off linearly with pressure from sea level (1010 hPa) to zero at the 900-hPa level. The mixing ratio of water vapor within this layer is 20 g $kg^{-1}$. Estimate the rainfall rate under the assumption that all the water vapor that converges into the ITCZ in the low level flow condenses and falls as rain.

***Answers:*** *(a) (b)*

7.8 Consider a velocity field that can be represented as

$$\mathbf{V}_\Psi = -\mathbf{k} \times \nabla\Psi$$

or, in Cartesian coordinates,

$$u_\Psi = -\partial\Psi/\partial y;\ v_\Psi = \partial\Psi/\partial x$$

where $\Psi$ is called the *streamfunction*. Prove that $\mathrm{Div}_H\,\mathbf{V}$ is everywhere equal to zero and the vorticity field is given by

$$\zeta = \nabla^2\Psi. \tag{7.43}$$

Given the field of vorticity, together with appropriate boundary conditions, the inverse of (7.22); namely

$$\Psi = \nabla^{-2}\zeta \tag{7.44}$$

may be solved to obtain the corresponding streamfunction field.[34] Because the true wind field at extratropical latitudes tends to be quasi-nondivergent, it follows that $\mathbf{V}$ and $\mathbf{V}_\Psi$ tend to be quite similar.

7.9 For streamfunctions $\Psi$ with the following functional forms, sketch the velocity field $\mathbf{V}_\Psi$. (a) $\Psi = my$, (b) $\Psi = my + n\cos 2\pi x/L$, (c) $\Psi = m(x^2 + y^2)$, and (d) $\Psi = m(xy)$ where $m$ and $n$ are constants.

7.10 For each of the flows in the previous exercise, describe the distribution of vorticity.

***Answers:*** *(a) and (d) are irrotational (i.e., vorticity free); (b)* $\zeta = -n(2\pi/L)^2 \cos 2\pi x/L$*; (c) exhibits uniform vorticity equal to 4m.*

7.11 Apply Eq.(7.5), which describes the advection of a passive tracer $\psi$ by a horizontal flow pattern to a field in which the initial conditions are $\partial\psi/\partial x = 0$ and $\psi = -my$. (a) Prove that at the initial time $t = 0$,

$$\frac{d}{dt}\left(\frac{\partial\psi}{\partial x}\right) = m\frac{\partial v}{\partial x} \quad \text{and} \quad \frac{d}{dt}\left(-\frac{\partial\psi}{\partial x}\right) = m\frac{\partial v}{\partial y}$$

Interpret this result, making use of Fig. 7.4. (b) Prove that for a field advected by the pure deformation flow in Fig. 7.4a, the meridional gradient $-\partial\psi/\partial y$ grows exponentially with time, whereas for a field advected by the shear flow in Fig. 7.4b, $\partial\psi/\partial x$ increases linearly with time.

7.12 Prove that for a flow consisting of pure rotation, the circulation $C$ around circles concentric with the axis of rotation is equal to $2\pi$ times the angular momentum per unit mass.

7.13 Extend Fig. 7.8 by adding the positions of the marble at points 13–24.

7.14 Consider two additional "experiments in a dish" conducted with the apparatus described in Fig. 7.7. (a) The marble is released from point $r_0$ with initial counterclockwise motion $\Omega r_0$ in the fixed frame of reference. Show that the orbits of the marble in both fixed and rotating frames of reference are circles of radius $r_0$, concentric with the center of the dish. (b) The marble is released from point $r_0$ with initial clockwise motion $\Omega r_0$ in the fixed frame of reference. Show that in the rotating frame of reference the marble remains stationary at the point of release.

7.15 Prove that for a small closed loop of area $A$ that lies on the surface of a rotating spherical planet, the circulation associated with the motion in an inertial frame of reference is $(f + \zeta)A$.

7.16 An air parcel is moving westward at 20 m $s^{-1}$ along the equator. Compute: (a) the apparent acceleration toward the center of the Earth from the point of view of an observer external

[34] Eq. (7.43) and (7.44) can be solved using finite difference techniques or Fourier transforms, as described in Section 7.3.5.

to the Earth and in a coordinate system rotating with the Eart, and (b) the apparent Coriolis force in the rotating coordinate system.

***Answer:*** *(a) $311 \times 10^{-4}$ and $0.627 \times 10^{-4}$ m s$^{-2}$; (b) $29.1 \times 10^{-4}$ m s$^{-2}$ downward*

7.17 A projectile is fired vertically upward with velocity $w_0$ from a point on Earth. (a) Show that in the absence of friction the projectile will land at a distance

$$\frac{4w_0^3\Omega}{3g^2}\cos\phi$$

to the west of the point from which it was fired. (b) Calculate the displacement for a projectile fired upward on the equator with a velocity of 500 m s$^{-2}$.

***Answer:*** *126 m*

7.18 A locomotive with a mass of $2 \times 10^4$ kg is moving along a straight track at 40 m s$^{-1}$ at 43 °N. Calculate the magnitude and direction of the transverse horizontal force on the track.

***Answer:*** *70 N to the right of the direction of movement*

7.19 Within a local region near 40 °N, the geopotential height contours on a 500-hPa chart are oriented east–west and the spacing between adjacent contours (at 60-m intervals) is 300 km, with geopotential height decreasing toward the north. Calculate the direction and speed of the geostrophic wind.

***Answer:*** $\mathbf{V}_g = 21.0$ *m s$^{-1}$ from the west*

7.20 (a) Prove that the divergence of the geostrophic wind is given by

$$\nabla \cdot \mathbf{V}_g \equiv \frac{\partial u_g}{\partial x} + \frac{\partial v_g}{\partial y} = \frac{v_g}{f}\frac{\partial f}{\partial y} = -v_g\frac{\cot\phi}{R_E}$$

$$= -v_g\frac{\cot\phi}{R_E} \qquad (7.45)$$

and give a physical interpretation of this result. (b) Calculate the divergence of the geostrophic wind at 45 °N at a point where $v_g = 10$ m s$^{-1}$.

***Answer:*** *$1.57 \times 10^{-6}$ s$^{-1}$*

7.21 Two moving ships passed close to a fixed weather ship within a few minutes of one another. The first ship was steaming eastward at a rate of 5 m s$^{-1}$ and the second northward at 10 m s$^{-1}$. During the 3-h period that the ships were in the same vicinity, the first recorded a pressure rise of 3 hPa while the second recorded no pressure change at all. During the same 3-h period, the pressure rose 3 hPa at the location of the weather ship (50 °N, 140 °W). On the basis of these data, calculate the geostrophic wind speed and direction at the location of the weather ship.

***Answer:*** $\mathbf{V}_g = 20$ *m s$^{-1}$ from the west*

7.22 At a station located at 43 °N, the surface wind speed is 10 m s$^{-1}$ and is directed across the isobars from high toward low pressure at an angle $\psi = 20°$. Calculate the magnitude of the frictional drag force and the horizontal pressure gradient force (per unit mass).

***Answer:*** *$3.63 \times 10^{-4}$ m s$^{-2}$ and $P_n = 1.06 \times 10^{-3}$ m s$^{-2}$*

7.23 Show that if frictional drag is neglected, the horizontal equation of motion can be written in the form

$$\frac{d\mathbf{V}}{dt} = -f\mathbf{k} \times \mathbf{V}_a \qquad (7.46)$$

where $\mathbf{V}_a \equiv \mathbf{V} - \mathbf{V}_g$ is the *ageostrophic* component of the wind.

7.24 Show that in the case of anticyclonic air trajectories, gradient wind balance is possible only when

$$P_n \leq f^2R_T/4$$

[**Hint**: Solve for the speed of the gradient wind, making use of the quadratic formula.]

7.25 Prove that the thermal wind equation can also be expressed in the forms

$$\frac{\partial \mathbf{V}_g}{\partial p} = -\frac{R}{fp}\nabla T$$

and

$$\frac{\partial \mathbf{V}_g}{\partial z} = -\frac{g}{fT}\nabla T$$

7.26 At a certain station, the 1000-hPa geostrophic wind is blowing from the northeast (050°) at 10 m s$^{-1}$ while the 700-hPa geostrophic wind is blowing from the west (270°) at 30 m s$^{-1}$. Subsidence is producing adiabatic warming at a rate of 3 °C day$^{-1}$ in the 1000 to 700-hPa layer and diabatic heating is negligible.

Calculate the time rate of change of the thickness of the 1000 to 700-hPa layer. The station is located at 43 °N.

***Answer:*** *Decreasing at a rate of 140 m day$^{-1}$*

7.27 (a) Prove that the geostrophic temperature advection in a layer of the atmosphere (i.e., the rate of change of temperature due to the horizontal advection of temperature) is given by

$$\frac{f}{R \ln (p_B/p_T)} V_{gB} V_{gT} \sin \theta$$

where the subscripts $B$ and $T$ refer to conditions at the bottom and top of the layer, respectively, and $\theta$ is the angle between the geostrophic wind at the two levels, defined as positive if the geostrophic wind veers with increasing height. (b) At a certain station located at 43 °N, the geostrophic wind at the 1000-hPa level is blowing from the southwest (230°) at 15 m s$^{-1}$ while at the 500-hPa level it is blowing from the west–northwest (300°) at 30 m s$^{-1}$. Calculate the geostrophic temperature advection.

***Answer:*** *18.3 °C day$^{-1}$*

7.28 Prove that in the line integral around any closed loop that lies on a pressure surface, the pressure gradient force $-\nabla\Phi$ vanishes, i.e.,

$$\oint \mathbf{P} ds = -\oint \nabla\Phi ds = 0 \qquad (7.47)$$

7.29 Prove that in the absence of friction (i.e., with the only force being the pressure gradient force), the circulation

$$C_a \equiv \oint \mathbf{c} \cdot ds \qquad (7.48)$$

is conserved, where $\mathbf{c}$ is the velocity in an inertial frame of reference.

7.30 Based on the result of the previous exercise, prove that in an inertial frame of reference

$$[c_s]\frac{dL}{dt} = -L\frac{d[c_s]}{dt}$$

where

$$[c_s] \equiv \frac{\oint \mathbf{c} \cdot ds}{L}$$

$[c_s]$ is the tangential velocity averaged over the length of the loop and $\mathrm{L} = \oint ds$ is the length of the loop. Hence, a lengthening of the loop must be accompanied by a proportionate decrease in the mean tangential velocity along the loop and vice versa.

7.31 For the special case of an axisymmetric flow in which the growing or shrinking loop is concentric with the axis of rotation, prove that the conservation of circulation is equivalent to the conservation of angular momentum. [**Hint**: Show that angular momentum $M = C/2\pi$.]

7.32 Starting with the horizontal equation of motion (7.14) and ignoring friction, derive a conservation law for vorticity $\zeta$ in horizontal flow on a rotating planet.

***Solution:*** We begin by rewriting the horizontal equation of motion (7.14) in Cartesian form, ignoring the frictional drag term

$$\frac{du}{dt} = -\frac{\partial\Phi}{\partial x} + fv \qquad (7.49a)$$

$$\frac{dv}{dt} = -\frac{\partial\Phi}{\partial y} - fu \qquad (7.49b)$$

Then we expand these expressions in Eulerian form, neglecting the vertical component of the advection, which is about an order of magnitude smaller than the corresponding horizontal advection terms

$$\frac{\partial u}{\partial t} = -u\frac{\partial u}{\partial x} - v\frac{\partial u}{\partial y} - \frac{\partial\Phi}{\partial x} + fv \qquad (7.50a)$$

$$\frac{\partial v}{\partial t} = -u\frac{\partial v}{\partial x} - v\frac{\partial v}{\partial y} - \frac{\partial\Phi}{\partial y} - fu \qquad (7.50b)$$

Differentiating (7.50a) with respect to $y$ and (7.50b) with respect to $x$, and subtracting the first from the second yields, after rearranging terms

$$\frac{\partial}{\partial x}\frac{\partial v}{\partial t} - \frac{\partial}{\partial y}\frac{\partial u}{\partial t} = -\frac{\partial u}{\partial x}\frac{\partial v}{\partial x} + \frac{\partial u}{\partial x}\frac{\partial u}{\partial x} - u\frac{\partial}{\partial x}\frac{\partial v}{\partial x} + u\frac{\partial}{\partial y}\frac{\partial u}{\partial x}$$
$$-\frac{\partial v}{\partial x}\frac{\partial v}{\partial y} + \frac{\partial v}{\partial y}\frac{\partial u}{\partial y} - v\frac{\partial}{\partial x}\frac{\partial v}{\partial x} + v\frac{\partial}{\partial y}\frac{\partial u}{\partial y}$$
$$-f\left(\frac{\partial u}{\partial x} + \frac{\partial v}{\partial y}\right) - v\frac{\partial f}{\partial y}$$

Reversing the order of differentiation of the terms on the left-hand side yields $\partial\zeta/\partial t$. The four

terms involving products of velocity derivatives can be rewritten in the more compact form

$$-\zeta\left(\frac{\partial u}{\partial x}+\frac{\partial v}{\partial y}\right)$$

and the four remaining terms in the two top lines as

$$-u\frac{\partial \zeta}{\partial x}-v\frac{\partial \zeta}{\partial y}$$

With these substitutions, we obtain

$$\frac{\partial \zeta}{\partial t}=-u\frac{\partial \zeta}{\partial x}-v\frac{\partial \zeta}{\partial y}-(f+\zeta)\left(\frac{\partial u}{\partial x}+\frac{\partial v}{\partial y}\right)-v\frac{\partial f}{\partial y}$$

Rearranging slightly (noting that $\partial f/\partial t = 0$) and reintroducing vector notation yields the conservation law

$$\frac{\partial}{\partial t}(f+\zeta)=-\mathbf{V}\cdot\nabla(f+\zeta)-(f+\zeta)(\nabla\cdot\mathbf{V})$$

or, in Lagrangian form,

$$\frac{d}{dt}(f+\zeta)=-(f+\zeta)(\nabla\cdot\mathbf{V})$$

These equations appear in the text as Eq. (7.21a,b). ■

7.33 Consider a sinusoidal wave along latitude $\phi$ with wavelength $L$ and amplitude $v$ in the meridional wind component. The wave is embedded in a uniform westerly flow with speed $U$. (a) Show that the amplitude of the geopotential height perturbations associated with the wave is $fvL/2\pi g$ where $f$ is the Coriolis parameter and $g$ is the gravitational acceleration. (b) Show that the amplitude of the associated vorticity perturbations is $(2\pi/L)v$. Show that the maximum values of the advection of planetary and relative vorticity are $\beta v$ and $(2\pi/L)^2Uv$, respectively, and that they are coincident and of opposing sign. (c) Show that the advection terms exactly cancel for waves with wavelength

$$L_s=2\pi\sqrt{\frac{U}{\beta}}.$$

$L_S$ is referred to as the wavelength of a stationary Rossby wave.

7.34 Suppose that the wave in the previous exercise propagating is along 45° latitude and has a wavelength of 4000 km. The amplitude of the meridional wind perturbations associated with the wave is 10 m $s^{-1}$ and the background flow $U = 20$ m $s^{-1}$. Assume that the velocity field is independent of latitude. Using the results of the previous exercise, estimate (a) the amplitude of the geopotential height and vorticity perturbations in the waves, (b) the amplitude of the advection of planetary and relative vorticity, and (c) the wavelength of a stationary Rossby wave embedded in a westerly flow with a speed of 20 m $s^{-1}$ at 45° latitude.

***Answers:*** *(a) 64.6 m; 1.57 × $10^{-5}$ $s^{-1}$ (b) 1.62 × $10^{-10}$ and 4.93 × $10^{-10}$ $s^{-2}$, respectively; and (c) 7000 km*

7.35 Verify the validity of the conservation of barotropic potential vorticity $(f + \zeta)/H$, as expressed in Eq. (7.27). [**Hint**: You might wish to verify and make use of the identity $dy/y = -dx/x$, where $y = 1/x$.]

7.36 Consider barotropic ocean eddies propagating meridionally along a sloping continental shelf, with depth increasing toward the east, as pictured in Fig. 7.28, conserving barotropic potential vorticity in accordance with (7.27). There is no background flow. In which direction will the eddies propagate? [**Hint**: Consider the vorticity tendency at points A and B]

***Answer:*** *Southward in the northern hemisphere; northward in the southern hemisphere.*

7.37 During winter in middle latitudes, the meridional temperature gradient is typically

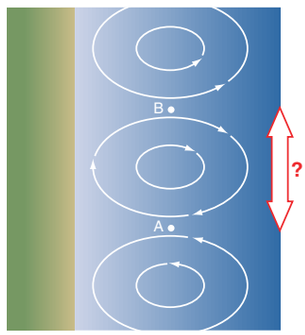


**Fig. 7.28** Barotropic ocean eddies propagating along a continental shelf, as envisioned in Exercise 7.36. Lighter blue shading indicates shallower water.

on the order of 1° per degree of latitude, while potential temperature increases with height at a rate of roughly 5 °C km$^{-1}$. What is a typical slope of the potential temperature surfaces in the meridional plane? Compare this result with the slope of the 500-hPa surface in Exercise 7.17.

***Answer:*** *$1.7 \times 10^{-3}$ versus $0.2 \times 10^{-3}$*

7.38 Making use of the approximate relationship $\omega \simeq -\rho g w$, show that the vertical motion term

$$\left(\frac{kT}{p} - \frac{\partial T}{\partial p}\right)\omega$$

in Eq. (7.37) is approximately equal to

$$-w\,(\Gamma_d - \Gamma)$$

where $\Gamma_d$ is the dry adiabatic lapse rate and $\Gamma$ is the observed lapse rate.

7.39 Figure 7.29 shows an idealized trapezoidal vertical velocity profile in a certain rain area in the tropics. The horizontal convergence into the rain area in the 1000 to 800-hPa layer is $10^{-5}$ s$^{-1}$, and the average water vapor content of this converging air is 16 g kg$^{-1}$. (a) Calculate the divergence in the 200 to 100-hPa layer. (b) Estimate the rainfall rate using the assumption that all the water vapor is condensed out during the ascent of the air.

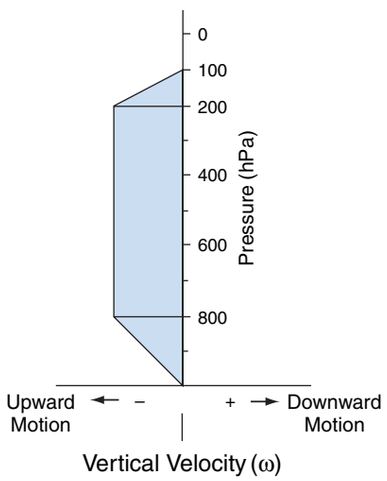


**Fig. 7.29** Vertical velocity profile for Exercise 7.39.

***Solution*** (a) Let $(\nabla \cdot \mathbf{V})_L$ and $(\nabla \cdot \mathbf{V})_H$ refer to the divergences in the lower and upper layers, respectively. Continuity of mass requires that

$$\int_{100}^{200} (\nabla \cdot \mathbf{V})_H \, dp = \int_{800}^{1000} (\nabla \cdot \mathbf{V})_L \, dp$$

Hence,

$$(\nabla \cdot \mathbf{V})_H = (\nabla \cdot \mathbf{V})_L \times \left(\frac{1000 - 800}{200 - 100}\right)$$
$$= 2 \times 10^{-5}\,\text{s}^{-1}.$$

(b)

$$\omega_{800} = -\int_{1000}^{800} (\nabla \cdot \mathbf{V})_L \, dp + \omega_{1000}$$
$$= (\nabla \cdot \mathbf{V})_L\,(1000\ \text{hPa} - 800\ \text{hPa}) + \omega_{1000}$$
$$= (-10^{-5}\,\text{s}^{-1})\,(200\ \text{hPa}) + 0$$
$$= -2 \times 10^{-3}\,\text{hPa s}^{-1}$$

Making use of the relationship $\omega \approx -\rho g w$, the vertical mass flux $\rho w$ can be obtained by dividing $\omega$ (in SI units) by $g$. Therefore, the rate at which liquid water is being condensed out is

$$\frac{2 \times 10^{-1}\ \text{Pa s}^{-1}}{(9.8\ \text{m s}^{-2})} \times 0.016$$
$$= 3.27 \times 10^{-6}\,\text{kg m}^{-2}\,\text{s}^{-1}$$

We can express the rainfall rate in more conventional terms by noting that 1 kg in$^{-2}$ of liquid water is equivalent to a depth of 1 mm. Thus the rainfall rate is $3.27 \times 10^{-4}$ mm s$^{-1}$ or

$$3.27 \times 10^{-1}\ \text{mm s}^{-1} \times 8.64 \times 10^{4}\ \text{s day}^{-1}$$
$$= 28.3\ \text{mm day}^{-1}$$

which is a typical rate for moderate rain. ■

7.40 In middle-latitude winter storms, rainfall (or melted snowfall) rates on the order of 20 mm day$^{-1}$ are not uncommon. Most of the convergence into these storms takes place within the lowest 1–2 km of the atmosphere (say, below 850 hPa) where the mixing ratios are on the order of 5 g kg$^{-1}$. Estimate the magnitude of the convergence into such storms.

***Answer:*** *$3 \times 10^{-5}\ s^{-1}$*

7.41 The area of a large cumulonimbus anvil in Fig. 7.30 is observed to increase by 20% over a 10-min period. Assuming that this increase in

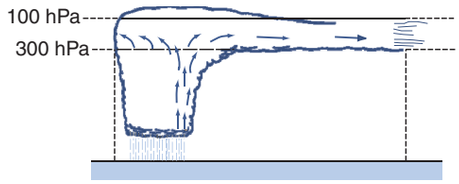


**Fig. 7.30** Physical situation in Exercise 7.41.

area is representative of the average divergence within the 300 to 100-hPa layer and that the vertical velocity at 100 hPa is zero, calculate the vertical velocity at the 300-hPa level.

***Solution*** From the results of Exercise 7.2,

$$\nabla \cdot \mathbf{V} = \frac{1}{A}\frac{dA}{dt} = \frac{0.20}{600\ \text{s}} = 3.33 \times 10^{-4}\ \text{s}^{-1}$$

Making use of (7.39), we have

$$\begin{aligned}\omega_{300} &= \omega_{100} - (\nabla \cdot \mathbf{V})\,(300 - 100)\ \text{hPa} \\ &= 0 - 3.33 \times 10^{-4}\ \text{s}^{-1} \times 200\ \text{hPa} \\ &= -6.66 \times 10^{-2}\ \text{hPa s}^{-1}\end{aligned}$$

To express the vertical velocity in height coordinates we make use of the approximate relation (7.32)

$$\begin{aligned}w_{300} &\simeq -\frac{\omega_{300}}{\rho g} = -\frac{\text{RT}}{pg}\omega_{300} = -\frac{H}{g}\omega_{300} \\ &\simeq \frac{7\ \text{km}}{300\ \text{hPa}} \times -6.66 \times 10^{-2}\ \text{hPa s}^{-1} \\ &\simeq 1.5\ \text{m s}^{-1}\end{aligned}$$

Note that this is the 300-hPa vertical velocity averaged over the area of the anvil. The vertical velocity within the updraft may be much larger. In contrast, divergences and vertical motions observed in large-scale weather systems are much smaller than those considered in this exercise. ■

7.42 Figure 7.31 shows the pressure and horizontal wind fields in an atmospheric Kelvin wave that propagates zonally along the equator. Pressure and zonal wind oscillate sinusoidally with longitude and time, while $v = 0$ everywhere. Such waves are observed in the stratosphere where frictional drag is negligible in comparison with the other terms in the horizontal equations of motion. (a) Prove that the waves propagate eastward. (b) Prove that the zonal wind component is in geostrophic equilibrium with the pressure field.

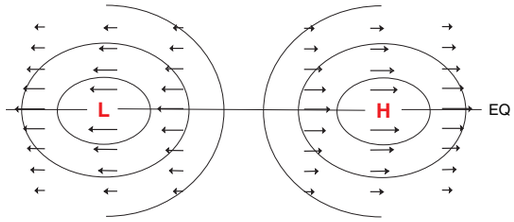


**Fig. 7.31** Distribution of wind and geopotential height on a pressure surface in an equatorial Kelvin wave in a coordinate system moving with the wave.

7.43 Averaged over the mass of the atmosphere, the root mean squared velocity of fluid motions is ~17 m s$^{-1}$. By how much would the center of gravity of the atmosphere have to drop in order to generate the equivalent amount of kinetic energy?

***Answer:*** *14.7 m*

7.44 Suppose that a parcel of air initially at rest on the equator is carried poleward to 30° latitude in the upper branch of the Hadley cell, conserving angular momentum as it moves. In what direction and at what speed will it be moving when it reaches 30°?

***Answer:*** *Eastward at 120 m s$^{-1}$*

7.45 On average over the globe, kinetic energy is being generated by the cross-isobar flow at a rate of ~2 W m$^{-2}$. At this rate, how long would it take to "spin up" the general circulation, starting from a state of rest?

***Answer:*** *About a week*

7.46 The following laboratory experiment provides a laboratory analog for the kinetic energy cycle in the atmospheric general circulation. The student is invited to verify the steps along the way and to provide physical interpretations, as appropriate.

A tank with vertical walls is filled with a homogeneous (constant density) incompressible fluid. The height of the undulating free surface of the fluid is $Z(x, y)$.

(a) Show that the horizontal component of the pressure gradient force (per unit mass) is independent of height and given by

$$\mathbf{P} = -g\nabla Z$$

(b) Show that the continuity equation takes the form

$$\nabla \cdot \mathbf{V} + \frac{\partial w}{\partial z} = 0$$

where $\mathbf{V}$ is the horizontal velocity vector and $w$ is the vertical velocity.

(c) Assuming that $\mathbf{V}$ is independent of height, show that

$$\frac{dZ}{dt} = -[Z]\,(\nabla \cdot \mathbf{V})$$

where [Z] is the mean height of the free surface of the fluid.

(d) Show that the potential energy of the fluid in the tank is

$$\frac{1}{2}\rho g \iint Z^2\, dA$$

and that the fraction of this energy available for conversion to kinetic energy is

$$\frac{1}{2}\rho g \iint Z'^2\, dA$$

where $Z'$ is the perturbation of the height of the surface from its area averaged height.

(e) Show that the rate of conversion from potential energy to kinetic energy is

$$-\rho g \iint Z' \frac{dZ'}{dt}\, dA$$

(f) If $Z'$ is much smaller than the mean height of the fluid, show that (e) is equivalent to

$$\rho g\,[Z] \iint Z'\,(\nabla \cdot \mathbf{V})\, dA$$

(g) Because the tank is cylindrical and fluid cannot flow through the walls,

$$\iint (\nabla \cdot \mathbf{V}Z')\, dA = 0$$

Making use of this result, verify that (f) can be rewritten as

$$-\rho g\,[Z] \iint (\mathbf{V} \cdot \nabla Z)\, dA$$

[AU1] Equation 7.43 is repeated twices in this chapter. Please check.